# NAVAL POSTGRADUATE SCHOOL
## Monterey, California


# THESIS

**INVESTIGATION INTO THE MECHANISM OF ACICULAR FERRITE NUCLEATION IN STEEL WELD METAL**

by

Michael F. Mahony

June 1999

Thesis Advisor: Alan G. Fox

**Approved for public release; distribution is unlimited.**

# REPORT DOCUMENTATION PAGE

Form Approved
OMB No. 0704-0188



| 1. AGENCY USE ONLY *(Leave blank)* | 2. REPORT DATE<br>June 1999 | 3. REPORT TYPE AND DATES COVERED<br>Master's Thesis |
|---|---|---|

**4. TITLE AND SUBTITLE:**
**INVESTIGATION INTO THE MECHANISM OF ACICULAR FERRITE NUCLEATION IN STEEL WELD METAL**

**5. FUNDING NUMBERS**

**6. AUTHOR(S)**
Mahony, Michael F.

**7. PERFORMING ORGANIZATION NAME(S) AND ADDRESS(ES)**
Naval Postgraduate School
Monterey, CA 93943-5000

**8. PERFORMING ORGANIZATION REPORT NUMBER**

**9. SPONSORING / MONITORING AGENCY NAME(S) AND ADDRESS(ES)**

**10. SPONSORING/MONITORING AGENCY REPORT NUMBER**

**11. SUPPLEMENTARY NOTES**
The views expressed here are those of the authors and do not reflect the official policy or position of the Department of Defense or the U.S. Government.

**12a. DISTRIBUTION / AVAILABILITY STATEMENT**
Approved for public release; distribution is unlimited.

**12b. DISTRIBUTION CODE**

**13. ABSTRACT** ***(maximum 200 words)*** Although steel with its high strength and toughness has been used extensively in all facets of construction, the joining of steels through welding has been problematic at best. The weld itself is the weakest part in any structure. This belief has been pervasive until recently when a microstructure called acicular ferrite was discovered. Acicular ferrite forms on non-metallic inclusions found within the weldment and when significant amounts are "grown", the weldment's toughness and strength approaches that of the steel-base plate. Unfortunately, the mechanism by which high level of acicular ferrite is nucleated in steel weld metal is unknown. This thesis is ground-breaking work in understanding this process and factors that can influence acicular ferrite formation. The present work has found that titanium-rich inclusions are the strongest acicular ferrite formers available, and goes on to suggest a new, undocumented compound may form if the proper amounts of titanium and aluminum within the weld are produced. The applications are far reaching as steel is used by all services for most all equipment.

| 14. SUBJECT TERMS | 15. NUMBER OF PAGES |
|---|---|
| Acicular Ferrite, Shielded Metal Arc Welding, C-Mn Steel Weldments, Non-Metallic Inclusions | 98 |
| | 16. PRICE CODE |

| 17.SECURITY CLASSIFICATION OF REPORT | 18.SECURITYCLASSIFICATION OF THIS PAGE | 19. SECURITY CLASSIFICATION OF ABSTRACT | 20. LIMITATION OF ABSTRACT |
|---|---|---|---|
| Unclassified | Unclassified | Unclassified | UL |

DUDLEY KNOX LIBRARY
NAVAL POSTGRADUATE SCHOOL
MONTEREY, CA 93943-5101



# INVESTIGATION INTO THE MECHANISM OF ACICULAR FERRITE NUCLEATION IN STEEL WELD METAL

Michael F. Mahony
Captain, United States Army
B. S., University of Rhode Island, 1988

Submitted in partial fulfillment of the
requirements for the degree of

**MASTER OF SCIENCE IN MECHANICAL ENGINEERING**

from the

**NAVAL POSTGRADUATE SCHOOL**
**June 1999**

# ABSTRACT

Although steel with its high strength and toughness has been used extensively in all facets of construction, the joining of steels through welding has been problematic at best. The weld itself is the weakest part in any structure. This belief has been pervasive until recently when a microstructure called acicular ferrite was discovered. Acicular ferrite forms on non-metallic inclusions found within the weldment and when significant amounts are "grown", the weldment's toughness and strength approaches that of the steel-base plate. Unfortunately, the mechanism by which high levels of acicular ferrite is nucleated in steel weld metal is unknown. This thesis is ground-breaking work in understanding this process and factors that can influence acicular ferrite formation. The present work has found that titanium-rich inclusions are the strongest acicular ferrite formers available, and goes on to suggest a new, undocumented compound may form if the proper amounts of titanium and aluminum within the weld are produced. The applications of this work are far reaching as steel is used by all services for most all equipment. If welding practices can be adopted to obtain maximum amounts of acicular ferrite given the welding process, the equipment can be stronger, tougher and last much longer than today's standards.

# TABLE OF CONTENTS

# ACKNOWLEDGMENT

I would like to express my sincere gratitude and appreciation to Dr. Alan G. Fox for his enthusiasm, humor, and guidance during the course of this thesis.

Special acknowledgment is due to Dr. Sarath Menon, Dr. Nagarajan Rajagopalan and Mr. Richard Hashimoto, for their contribution of many hours of laboratory assistance.

Finally, I would like to thank my parents, Owen and Teresa, and my family, Norma, Kaitlin, Michaela, and Joseph, who provided the most important things of all, love and support.

# I. INTRODUCTION

Since the days of the earliest humans, acquisition and refinement of materials was a catalyst for the development and advancement of civilizations. The Bronze Age brought about huge increases in not just the number of different materials developed, but the level by which these materials were produced and manipulated for a common purpose. Steel with its excellent material properties, has been woven into every aspect of society today. Of all metals it is historically the most studied in its manufacturing, processing, and performance. Despite enormous successes in manufacturing high quality steel, the effective joining by welding has proven to be most difficult.

In order to produce weldments with similar strengths and toughness to the base plate metal, great care in controlling the welding process and welding consumables must be achieved. It has long been known a ferritic steel weld microstructure dominated by acicular ferrite increases the yield strength and toughness of the weld. To control the complex process of acicular ferrite nucleation given the specific weld process is thus of critical importance.

Any arc welding method used to join steel, be it shielded metal arc (SMAW), submerged arc (SAW), or gas metal arc (GMA), can lead to a microstructure containing combinations of the microstructural constituents: bainite, martensite, grain boundary ferrite, side plate ferrite, and acicular ferrite. Of these microconstituents, only acicular ferrite, if present in significant amounts, greatly improves the strength and toughness of the weld metal. Acicular ferrite nucleates intragranularly on nonmetallic inclusions

producing a fine "basket-weave" microstructure that is very resistant to crack propagation.

It is well known that nonmetallic inclusions in the weld metal are responsible for the nucleation of acicular ferrite. Many experiments have been performed to try and understand the relationship between these inclusions and the nucleation of acicular ferrite, but little information has been produced due to the complexity of the chemical interfaces involved.

The intention of the present work is to lead to a deeper understanding of the mechanism of acicular ferrite nucleation in C-Mn steel weld metal by performing new, novel methods of SEM and analytic TEM work proposed by Fox and Menon [Ref. 46]. This approach provides new and useful information to help in the development of filler wires for ferritic steels.

# II. BACKGROUND

## A. SHEILDED METAL ARC WELD PROCESS

Shielded metal arc welding (SMAW) is used extensively for maintenance, repair, and construction. Of all the arc welding processes, it is simple, portable, and relatively inexpensive. It joins metals by using the heat produced from a covered consumable electrode containing various filler metal and layered fluxes. A sketch of the SMAW process is shown in Figure 2-1. The electrode is usually baked to remove any excess moisture and hydrogen. This lowers the hydrogen in the electrode and, along with the gaseous shield produced by the arc, reduces the susceptibility of hydrogen embrittlement within the weld. The electrode, depending on the flux covering composition used, can perform one or more of the following functions [Ref. 1]:

- Provide a gaseous shield to protect the weld pool.
- Provide deoxidizers to clean the weld.
- Provide arc stabilizers to maintain a stable arc during welding.
- Provide alloying elements to the weld pool.

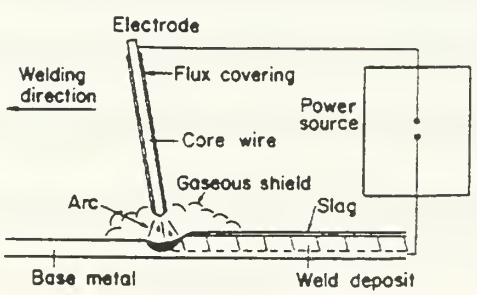


**Figure 2-1**. Sketch of shielded metal arc welding process [From Ref. 1].

## B. WELD METAL

### 1. General Microstructure

A sketch of a typical single pass, steel weld microstructure is shown in Figure 2-2. The overall weld can be broken into three regions: the fusion zone, the heat affected zone (HAZ), and the base metal. The HAZ is further subdivided into three more regions: grain coarsening, grain refining, and partial grain refining [Ref. 1].

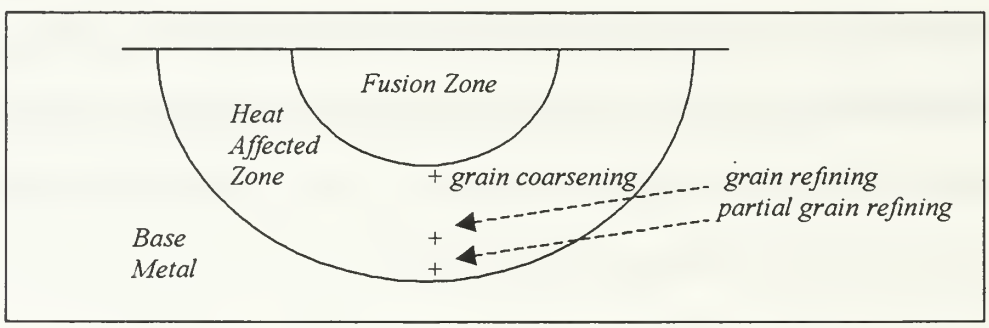


**Figure 2-2**. Sketch of single pass weld microstructure [Ref. 1].

The fusion zone is formed upon weld metal solidification. The microstructure and grain size in this zone are determined by epitaxial and competitive growth, the welding parameters used, and the weld metal composition [Ref. 1]. The grains grow from the unmelted part of the base metal (substrate) toward the center of the weld. The maximum thermal gradient during solidification is perpendicular to the solid/liquid interface, resulting in long columnar grains in the final fusion zone microstructure. Figure 2-3 shows a sketch of how the final fusion zone microstructure normally appears.

This microstructure can be highly susceptible to solidification cracking, particularly if the carbon and sulfur contents of the weld metal are high.

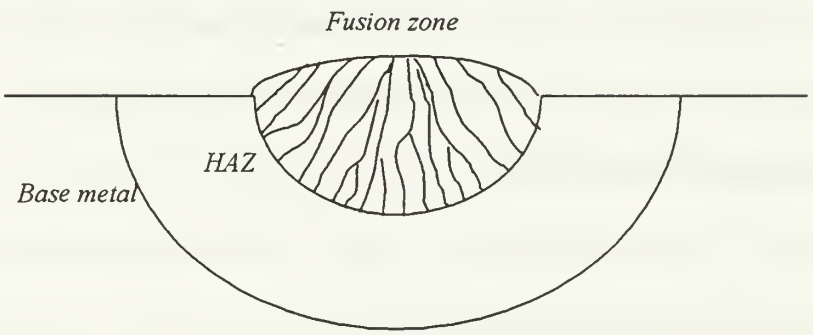


**Figure 2-3**. Sketch of typical fusion zone microstructure.

The Heat Affected Zone (HAZ) is the most complex area within the weld metal. If one takes into account the wide range of temperatures experienced between the base metal and the molten weld, coupled with the effects of multiple weld passes, the resulting microstructure and the number of continuous cooling transformation (CCT) diagrams required to describe this area would be enormous and impossible to generate [Ref. 6].

The Partial Grain Refining region in the HAZ, being closest to the base metal, experiences a temperature that reaches a level where some transformation to austenite occurs. Upon cooling, fine grains of pearlite and ferrite are formed.

The Grain Refining region in the HAZ is exposed to higher temperatures creating more opportunity for austenite nucleation, but not high enough temperatures to produce

coarsening. Upon cooling, very fine grains result producing the toughest microstructure in the weldment.

The Grain Coarsening region in the HAZ is exposed to the highest temperatures in the HAZ promoting coarsening of austenite grains. These grains are still smaller than the long columnar grains in the fusion zone. The cooling rates in this region can lead to the formation of untempered bainite and martensite. This together with the large grain size can lead to poor HAZ toughness.

### 2. Microstructural Constituents

The nomenclature of microstructural constituents in ferritic steel weld metals is highly diverse. Bhadeshia [Ref. 2] stated it best, "There are some difficulties with notation, which is derived largely from morphological observations rather that from the details of mechanism, which are more relevant for quantitative work." The International Welding Society established a guideline for optical classification of steel weld metal microstructural constituents [Ref. 3]. The guidelines for microstructural constituents are as follows:

#### *a. Primary Ferrite (PF)*

Solidification in steel weld deposits begins with the epitaxial growth of primary ferrite [Ref. 2]. Two forms of primary ferrite are possible: grain boundary ferrite and intragranular polygonal ferrite. Grain boundary ferrite, sometimes called allotriomorphic ferrite, nucleates at the prior austenite grain boundaries, while intragranular polygonal ferrite forms within the prior austenite grains. Both forms

depend on the diffusion of carbon into the austenite for growth with a Kurdjumov and Sachs orientation relationship [Ref. 4]. Formation of primary ferrite is usually associated with high temperatures and slow cooling rates.

### *b. Acicular Ferrite (AF)*

Acicular Ferrite is formed intragranularly, similar to intragranular polygonal ferrite, but the nucleation process and morphology are quite different. It nucleates on nonmetallic inclusions within the prior austenite grains, resulting in short ferrite needles with a basket-weave structure [Ref. 1]. The interlocking nature of the microstructure, together with fine grain size, produces a microstructure that is highly resistant to crack propagation. Lower temperatures with higher cooling rates are usually associated with acicular ferrite formation.

### *c. Ferrite with Second Phase (FS)*

This microstructural constituent includes both ferrite with aligned second phase and ferrite with nonaligned second phase. The ferrite with aligned second phase is normally referred to as Widmanstätten (side-plate) ferrite, upper bainite and lower bainite depending on morphology distinctions that are made using a scanning or transmission electron microscope. Differentiation between these phases is difficult using optical microscopy. Widmanstätten ferrite is associated with lower temperatures and faster cooling rates compared with primary ferrite. As the amount of undercooling is increased, the planar growth (allotriomorphic) mode can no longer be maintained due to the

relatively slower rate of carbon distribution [Ref. 5]. Ferrite sideplates are formed as a re-distribution of carbon along the sides of the advancing interface insues. Upper bainite forms at relatively higher temperatures (but lower than that required for side plate ferrite formation) with carbide particles situated between ferrite laths, while lower bainite forms at lower temperatures with the carbide particles precipitated within the ferrite laths.

### *d. Ferrite Carbide Aggregate (FC)*

Ferrite carbide aggregates form at high temperatures with relatively long cooling rates. Pearlite falls into this category. Ferrite and cementite form alternating layers or lamallae to produce colonies of pearlite. Due to the faster cooling rates associated with most welding processes (an exception is submerged arc welding), the ferrite carbide aggregate morphology is not normally found in steel weld metals (see Figure 2-4).

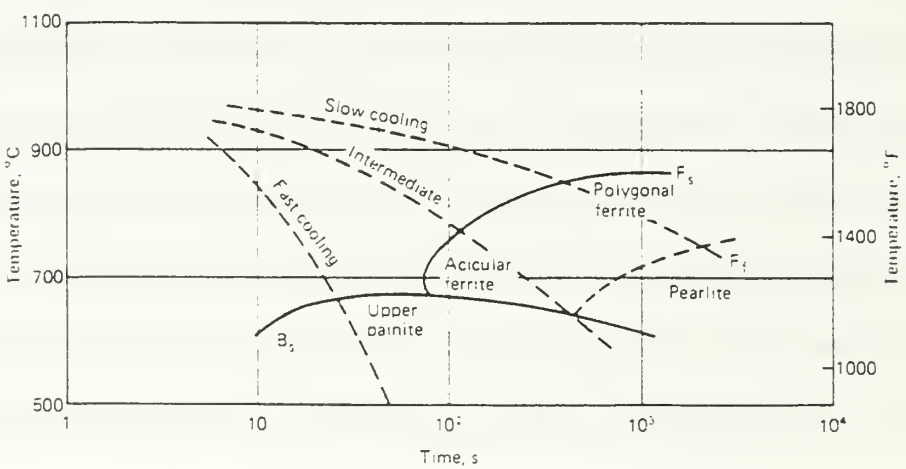


**Figure 2-4**. CCT diagram for a low-alloy steel weld metal [Ref 7].

### 3. Multipass Effects

Determining the weakest point in the weld, where brittle fracture is most likely to occur, for a single pass weld is not difficult. To determine the same information after multiple passes can be next to impossible. Figure 2-5 is a sketch of a typical multiple pass weld macrostructure. The continually process of heating and cooling has many effects on the overall microstructure. Depending on a region's peak temperature experienced, complete transformation, partial transformation, or a tempering effect can take place from pass to pass. Evans [Ref. 8] suggested that the toughness of multipass weld metal increases with increasing ratios of reaustenitized weld metal to total weld area. Much modeling and experimental work has been done to evaluate the effects of thermal cycles on weld metal toughness, but to date, the "weakest link" in a multipass weld metal is still a complex function of chemical composition, thermal history, and microstructural properties. However, regions associated with large columnar grains that are not subsequently reaustenitized are likely to be candidate areas for poor mechanical properties.

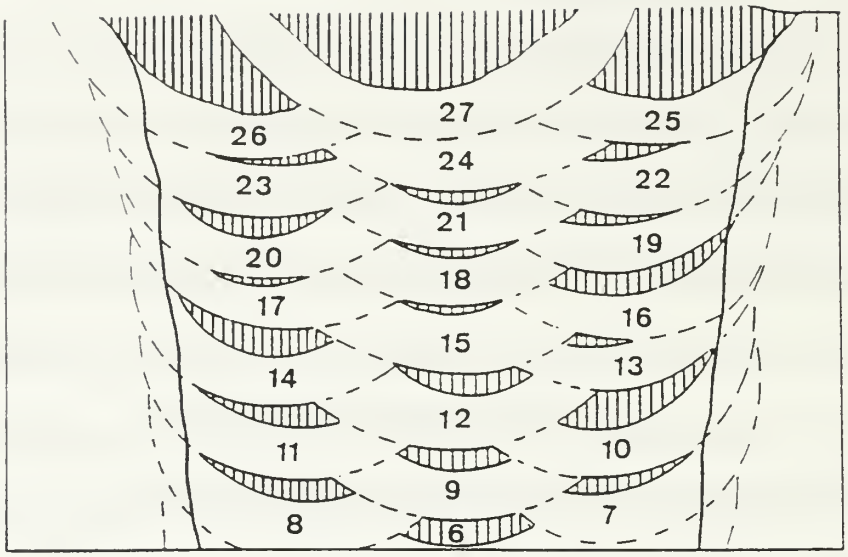


**Figure 2-5**. Multipass macrostructural appearance of a 27 pass weld metal [Ref. 7].

### 4. Control of Weld Microstructure

The title of this section is a little misleading as complete control of any multipass weld metal microstructure is near impossible. However, there are factors that can greatly effect the weld microstructure. The strength and toughness of ferritic steel weld metal depends on the following: (i) weld metal chemistry, (ii) welding process and heat input, (iii) weld metal continuous cooling characteristics and (iv) weld metal microstructure including precipitates and nonmetallic inclusions [Ref. 11]. The weld metal microstructural transformation depends on (1) the alloy content, (2) concentration, size distribution, and chemical composition of nonmetallic inclusions, (3) the solidification microstructure, (4) the prior austenite grain size, and (5) the heat input and deoxidation process [Ref. 12]. Of all these the one common theme associated with increasing

strength and toughness of a weld metal is the formation and microstructural domination of acicular ferrite throughout or at least when a pass is initially laid down. Figure 2-6 is a schematic CCT diagram displaying the effects of increasing heat input, increasing alloying elements, and decreasing oxygen content within the weld metal.

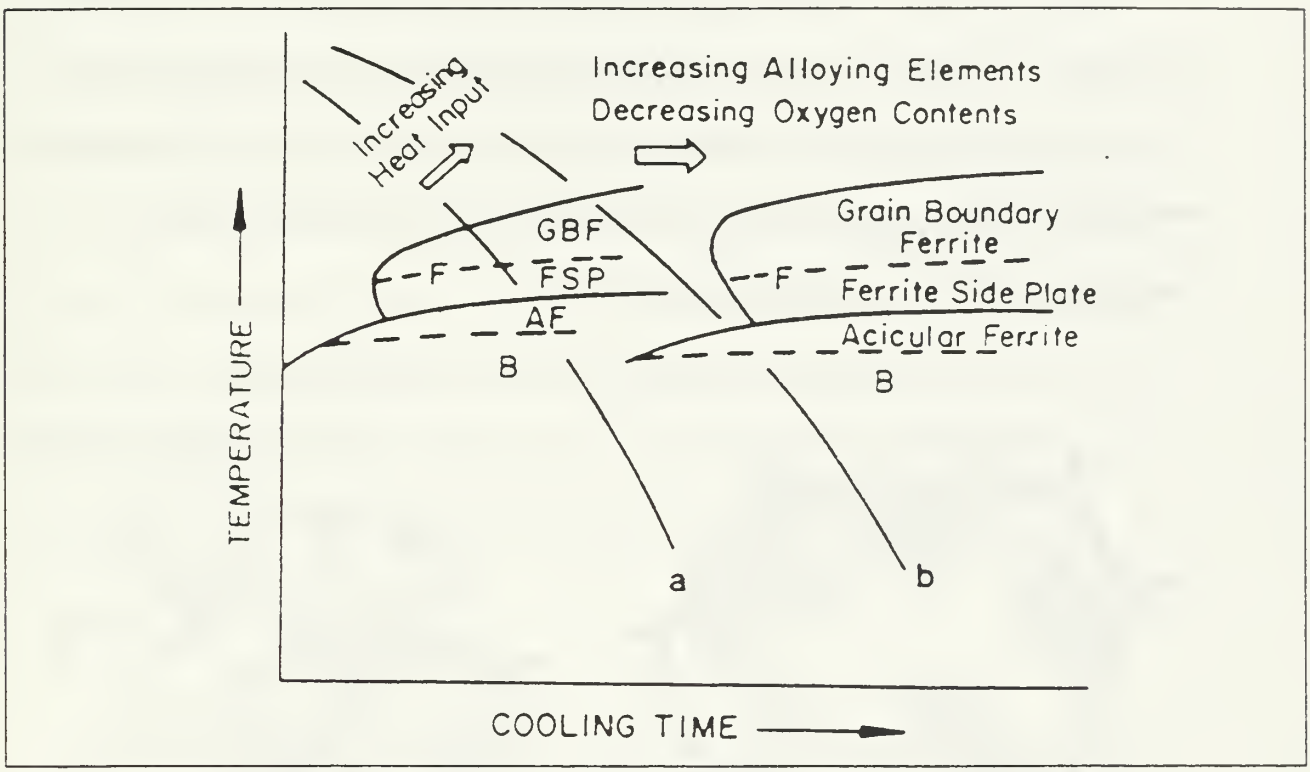


**Figure 2-6**. CCT diagram showing effects of increasing heat input and alloying [Ref. 1].

## C. THE NATURE OF ACICULAR FERRITE

Up until the last 25 years, acicular ferrite and bainite were terms used interchangeably. In fact, most work today [Ref. 9, 10, 11, 13] indicates that acicular ferrite is essentially intragranularly nucleated bainite. The difference, beside the obvious morphological appearance, is how and where these microconstituents nucleate. Bainite

nucleates at prior austenite grain boundaries and grows in organized packets, while acicular ferrite nucleates heterogeneously on nonmetallic inclusions and grows in many different directions [Ref. 15]. For larger austenite grain sizes, intragranular nucleation on nonmetallic inclusions dominates (if sufficient inclusions are present), so acicular ferrite is produced. For smaller austenite grains bainite predomintes, but if a subsequent heat treatment leads to an increased austenite grain size then acicular ferrite may form instead provided the inclusion size distribution is appropriate. Figure 2-7 depicts a sketch of the transition from bainite to acicular ferrite [Ref. 13].

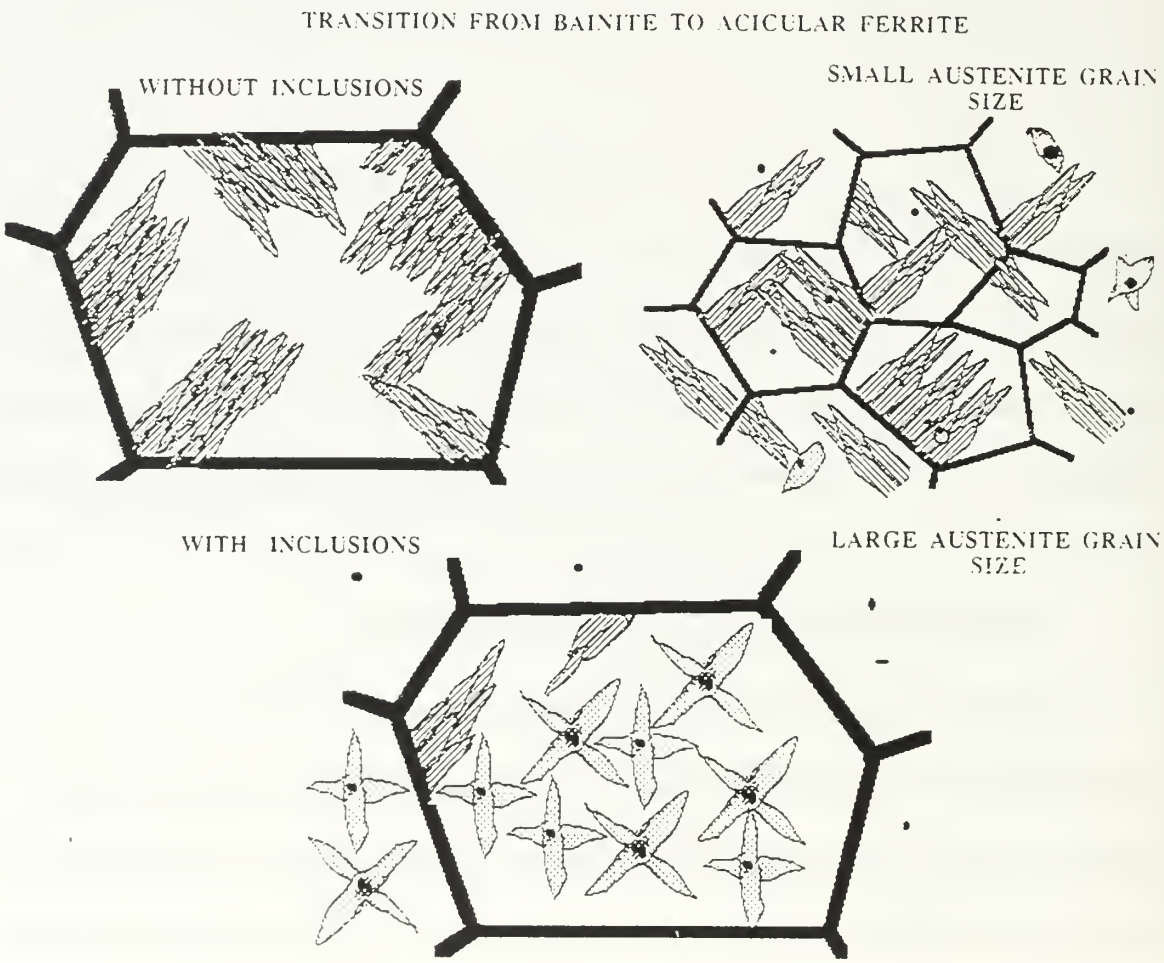


**Figure 2-7.** Sketch of the transition from bainite to acicular ferrite [Ref. 13].

### 1. Morphology

The term acicular means shaped and pointed like a needle [Ref. 2]. Acicular ferrite is formed intraganularly in the shape of short ferrite needles (in two dimensional sections) that together give an interlocking basket-weave feature. Plates of acicular ferrite do not cross austenite grain boundaries and all evidence indicates that its growth is diffusionless, with carbon partitioning into the austenite after transformation [Ref. 9].

Formation, nucleation, and growth of acicular ferrite requires the presence of nonmetallic inclusions. It is the ability of these nonmetallic inclusions to nucleate and grow acicular ferrite that will determine the strength and toughness of the weld metal. Efficiency of acicular ferrite nucleation from inclusion to inclusion changes based on a complex function of mechanisms that, to date, are not all together agreed upon.

### 2. Mechanism of Growth

The growth mechanisms discussed below relate to the growth of acicular ferrite on nonmetallic inclusions. It is believed that more than one, perhaps all, mechanisms of nucleation are responsible for acicular ferrite formation.

#### *a. Heterogeneous Nucleation by a Simple Substrate*

Although all indications point to heterogeneous nucleation of acicular ferrite on nonmetallic inclusions as the mechanism of growth, the belief that this is the only mechanism in effect is misguided. In fact, experimental theory predicts that the energy required to nucleate ferrite is much lower at prior austenite grain boundaries than

the surface of an inclusion [Ref. 16]. It is for this reason that simple heterogeneous nucleation of acicular ferrite alone is possible but less likely. It is important to note that if this is the only mechanism operating, the larger the inclusions the more effective they should be. Most work suggests a thin layer of allotriomorphic ferrite at the grain boundaries is required to promote the intragranular formation of acicular ferrite [Ref. 13]. The reason for this is because a build-up of carbon at the allotriomorphic ferrite and prior austenite interface prevents the progress of this grain boundary-nucleated ferrite so that acicular ferrite formation is then preferred.

### *b. Nucleation by Epitaxy*

According to lattice matching theory, nucleation can also occur if the crystallographic planes of both the substrate and the nucleant are similar [Ref. 15]. Lattice matching is a very popular explanation to describe the mechanism of nucleation of acicular ferrite by nonmetallic inclusions [Ref. 12]. It requires the inclusions to have crystal surfaces that are suitably oriented to "match" with ferrite; this reduces the energy required for nucleation. Depending on the inclusion, its plane of epitaxy and orientation, the affinity for acicular ferrite nucleation varies. Grong et al. [Ref. 14] indicate that appropriate nonmetallic inclusions must be cubic such as TiC, TiN, TiO, $MnO.Al_2O_3$, or $\alpha$-$Al_2O_3$ with good lattice matching to be effective acicular ferrite nucleants.

### *c. Strain Energy*

Normally inclusions have a lower thermal expansion coefficient than the surrounding matrix, and upon solidification, contraction strains develop around the inclusion [Ref. 15]. It has been suggested [Ref. 17, 18, 25] that these strains may be relieved by the transformation of austenite to ferrite in the area adjacent to the inclusion. Thermal expansion coefficients for various weld metal inclusions lend credence to this idea, but again this is unlikely to be the sole mechanism of nucleation since calculations suggest that such strains are small. In fact, it has also been suggested [Ref. 19, 20] that the differential thermal strain effect generated during welding is not a major factor in generation of steel weld metal microstructures (in particular acicular ferrite).

### *d. Interface Effects*

Chemical bonding and/or segregation at inclusion-ferrite interfaces within the weld metal is also a possible mechanism for growth of acicular ferrite. Mizuno et al. [Ref. 24] suggested that the strength of the bonding between a nonmetallic inclusion and the nucleated ferrite may be important. Gregg and Bhadesia [Ref. 15] concluded from their observations that chemical reactions at inclusion/matrix interfaces were a major mechanism for accelerated acicular ferrite formation and growth. The idea here is that some titanium oxide-containing inclusions ($TiO_2$ and $Ti_2O_3$) react with the surrounding matrix to form TiO and produce a local alloy depletion area (due to deoxidation)

of acicular ferrite nucleation from these inclusions due to the reduced hardenability of the weld metal immediately surrounding them.

## D. NONMETALLIC INCLUSIONS

### 1. General

For years the presence of nonmetallic inclusions in steels and steel weld metals were considered undesirable as they lowered the overall toughness of the steel/weld metal. In fact, much steel work over the past twenty years has been to manufacture high strength, high toughness steels devoid of inclusions (mostly sulfides and oxides). Production of "clean" weld metal with low oxygen levels is difficult because, in many welding processes, fluxes and cover gases lead to high weld metal oxygen contents (>200ppm). With the discovery of acicular ferrite nucleation by nonmetallic inclusions and its beneficial properties, the focus of work in the field today is identifying which nonmetallic inclusions are responsible for appreciable levels of acicular ferrite and by what mechanism nucleation is achieved.

### 2. Deoxidation

The process of deoxidation reduces the amount of oxygen and improves the toughness of the weld. The way this is done is by introducing oxide-forming elements within the weld pool. The dissolved oxygen reacts with these elements to form nonmetallic (oxide) inclusions. Hence, after the welding and solidification process, the amount of dissolved oxygen within the weld is reduced [Ref. 26]. The addition of

deoxidants such as Al, Ti, Si, and Mn in the filler metal will not only rid the weld metal of dissolved oxygen, but also helps to reduce the amount of carbon monoxide gas that leads to porosity in the fusion zone [Ref. 1].

### *a. Aluminum*

Of all the deoxidizing elements available, aluminum, with its large negative free energy to form oxides, is the most effective [Ref. 28, 32]. If aluminum is present in significant amounts ( $\geq 0.02$ wt), it will remove large amounts of oxygen and form aluminum-containing oxides (based on $Al_2O_3$) [Ref. 27]. In addition, previous work has shown aluminum oxides are effective acicular ferrite nucleators [Ref. 24, 26].

### *b. Titanium*

Titanium is the next strongest deoxidant usually occurring in different forms including TiO, $TiO_2$, and $Ti_2O_3$ [Ref. 27, 29, 30]. The actual titanium oxide that is the most effective acicular ferrite former is a topic of much debate; this will be discussed in the next major section.

### *c. Silicon*

Although a weak deoxidant, silicon in its oxide form, $SiO_2$, has been shown to be an effective acicular ferrite nucleator [Ref. 31]. Silicon by itself can decrease the toughness of the weld if found in appreciable quantities ($\geq 0.3\%$) [Ref. 1].

### *d. Manganese*

Also a weak deoxidant, manganese forms complex oxides that promote acicular ferrite formation. These nonmetallic oxides, usually in the form of $MnO.SiO_2$ and $MnO.Al_2O_3$, can nucleate acicular ferrite at the expense of grain boundary ferrite [Ref. 21]. Manganese will also react with any remaining sulfur and form MnS (see next section) that limits solidification cracking and thus increases toughness [Ref. 1].

## 3. Desulfurization

Like oxygen, sulfur is extremely difficult to totally eliminate from steel weld metal. In Mn-free steels sulfur will readily react with iron and form FeS that can significantly raise the susceptibility of solidification cracking [Ref. 1]. FeS forms films at the grain boundaries due to the associated low surface tension levels. If the manganese to sulfur content ratio in the weld metal is high enough (~ 12:1), MnS forms as globules instead and these do not wet the grain boundaries and thus decreases the susceptibility to solidification cracking. Copper can also combine with sulfur to form CuS and/or $Cu_2S$ if Mn is behaving as a significant deoxidant; these sulfides are also not as deleterious as FeS in the weld metal.

Some research has suggested that manganese sulfide-containing inclusions are effective at nucleating acicular ferrite. In fact, Yamamoto et al. [Ref. 48] have argued that MnS, which has been found to grow on titanium oxide inclusions, is responsible for the nucleation of acicular ferrite. Chijiiwa et al. [Ref. 49] and Abson [Ref. 21] dismiss this claim and believe sulfides actually lower the ability of inclusions to nucleate acicular

this claim and believe sulfides actually lower the ability of inclusions to nucleate acicular ferrite. Whether they have an influence in the nucleation process or not, sulfides have been found on many acicular ferrite-forming oxide inclusions as "caps" [Ref. 13, 39, 50] of MnS and CuS.

## E. PREVIOUS WORK

A great amount of work has been done over the years to understand the nonmetallic inclusions' role in the nucleation of acicular ferrite. Although strong acicular ferrite forming inclusions have been identified, the mechanism by which they nucleate and grow acicular ferrite is not generally agreed on.

### 1. Inclusions Thought to Nucleate Acicular Ferrite

The nucleation of acicular ferrite by nonmetallic inclusions has been observed by many workers [Ref. 21, 16, 13, 8, 5, 10, 11] and theoretical calculations performed [Ref. 16]. These support the notion that once the grain boundary sites for nucleation of ferrite have been saturated, the next favorable site is on nonmetallic inclusions. The larger the grain size the more likely is nucleation on inclusions.

Several specific phases in inclusions have been proposed as responsible for the nucleation of acicular ferrite. Zhang and Farrar [Ref. 40] concluded from their studies of several low alloy steels that TiO, $Al_2O_3$, $SiO_2$, MnO-$SiO_2$, TiO ($Al_2O_3$)-MnO-$SiO_2$, MnS and CuS can all nucleate acicular ferrite. Babu et al. [Ref. 13] provided some agreement with these results with the prediction of $MnO.Al_2O_3$ (galaxite), $Al_2O_3$, $TiO_2$, $Ti_3O_5$, $SiO_2$

and MnO inclusions in their theoretical calculations. A nucleation rate curve for these phases is displayed in Figure 2-8.

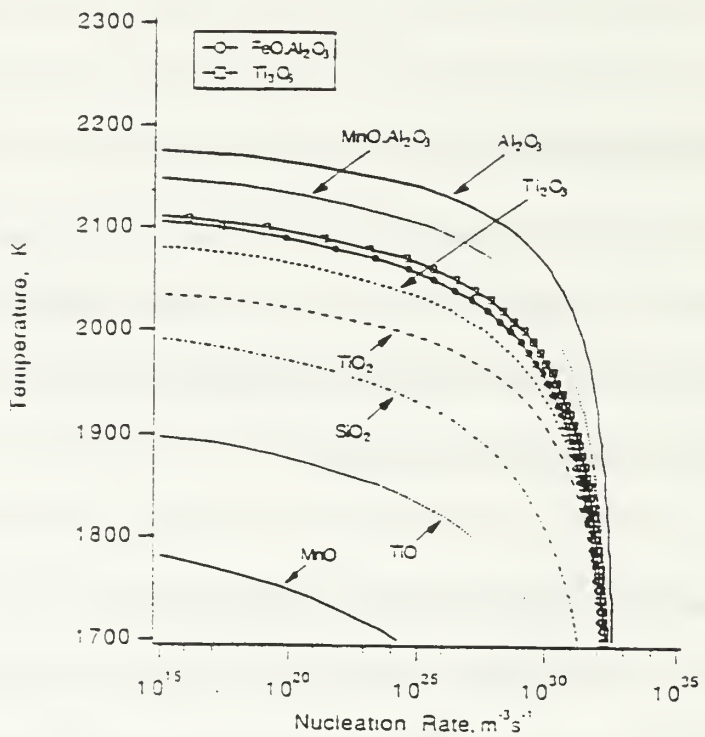


**Figure 2-8**. Nucleation rate curve generated using reaction equations [From Ref. 13].

There is conflicting results on the effectiveness of $\alpha$-$Al_2O_3$ for nucleating acicular ferrite. Mills [Ref. 34], Thewlis [Ref. 35], Cochrane [Ref. 35], and Saggese [Ref. 37] all concluded from their work that inclusions rich in aluminum favor a high percentage of acicular ferrite. Devillers [Ref. 23], Terashima and Hart [Ref. 37], and Grong and Matlock [Ref. 38] reported that inclusions containing high levels of $\alpha$-$Al_2O_3$ are *not*

beneficial to the formation of acicular ferrite. It is important to point out here that the inclusions in Saggese's work also contained a significant amount of TiO.

Fox, Eakes and Franke [Ref. 32] found inclusions containing MnO, $\alpha$-$Al_2O_3$, $SiO_2$ and a titanium-rich oxide in their HY-100 steel weld studies which led them to believe that galaxite, $MnO.Al_2O_3$, and pyrophanite, $MnO.TiO_2$, were the major components of these inclusions. Most workers in the field have found a titanium-rich phase within the inclusions but were unable to identify the phase as TiN, TiO or TiC because of the similar lattice parameters of these phases [Ref. 11-15, 23, 32-35]. St-Laurent and L'Esperance [Ref. 41] strongly suggest this titanium-rich phase is TiO.

### 2. Mechanisms of Acicular Ferrite Growth

As discussed earlier, acicular ferrite is essentially intragranularly nucleated bainite, exhibiting the same incomplete reaction phenomenon. In fact, it seems that bainite and acicular ferrite are in competition for nucleation and growth. Ito, Nakanishi and Komizo [Ref. 10] showed that as the oxygen concentration and volume fraction of oxide inclusions increases, the microstructure containing bainite is replaced by acicular ferrite. Thus, besides the obvious differences in morphology, acicular ferrite requires nonmetallic inclusions in relatively large austenite grains to nucleate, while bainite nucleates at prior austenite grain boundaries in steels that are relatively free of inclusions. So, as Bhadesia [Ref. 9] and many others have pointed out, under identical isothermal transformation conditions in the same inclusion rich steel, when the austenite grain sizes

are small, bainite nucleates at the grain boundaries. For large austenite grains, acicular ferrite forms as the number density of intragranular nucleation sites increase.

Because of the chemical complexity of the inclusions and the difficulty in conducting controlled experiments, identifying the exact mechanism of acicular ferrite growth is difficult at best. One of the major tools available to analyze these inclusions and their phases is the transmission electron microscope (TEM). Most analyses of inclusions have been accomplished through analytical modeling, energy dispersive x-ray (EDX), and electron diffraction. Recently, parallel electron energy loss spectroscopy (PEELS) has been used to study inclusions [Ref. 39]. The results from all this work have been inconclusive and the exact chemistry and crystallography of these acicular-ferrite-forming inclusions is still not wholly understood. For example, Zhang and Farrar [Ref. 40] showed evidence that all varieties of inclusions, whether oxides, nitrides, or sulfides, have the ability to nucleate acicular ferrite, but the reasons behind their vast differences in effectiveness is questionable.

If Zhang and Farrar [Ref. 40] are correct in their hypothesis that all inclusions are capable of nucleating acicular ferrite as simple substrates, then the number and average size of the inclusions will primarily determine their effectiveness as nucleants. This means that the inclusions' nucleation potency is solely based on the energy of the interfaces between the various types of inclusions and the ferrite formed. In fact, TiC, TiN and TiO, which all have the same crystal structure, have been shown recently to be effective acicular ferrite formers. But, Zhang, Hattori, and Tarui [Ref. 47] have suggested that of the three, TiC is the most effective and TiO the least effective at

nucleating acicular ferrite. These results suggest that it is the interface energy between the inclusion and the steel matrix that determines the nucleation potency, although there is significant evidence that epitaxial growth of acicular ferrite from TiO and TiN is also possible. Indeed, inclusions that display the best "'lattice matching" have long been thought to be the best acicular ferrite formers. Mills, Thewlis and Whiteman [Ref. 34] analyzed this idea in detail and suggest that there can be reproducible orientation relationships that generate high levels of acicular ferrite. It should be noted here that TiN has a greater disregistry with ferrite than TiO and TiN has been suggested as a stronger nucleant than TiO [Ref. 24], which suggests that simple lattice matching is not the only nucleation mechanism and the strength of nucleant bonding may be important as well. The discussion above indicates that, for lattice matching, the nucleating phases in the inclusions must be cubic and have a Bain orientation relationship to act as catalysts for acicular ferrite nucleation.

Inclusions form randomly oriented in space in the weld and only a certain number will thus be oriented appropriately with respect to both the austenite and the ferrite at the inclusion/acicular ferrite interface. Despite this random nature of the inclusions' orientations, Grong et al. [Ref. 12] made calculations that suggest that as many as 12% of the inclusions could produce the necessary orientation within the Bain region completely by chance. Further transmission electron microscopy work by Grong et al., found that the nucleant phases TiN, $\alpha$-$Al_2O_3$ and $MnO.Al_2O_3$ could have proper orientation with the Bain region. This lattice matching premise may help to explain why MnS and $MnO.SiO_2$, which cannot match with $\alpha$-Fe, are less effective at nucleating acicular ferrite

ferrite than $Al_2O_3$ and TiN. The inclusions should also have a slightly angular or "faceted" appearance and exhibit atomic arrangement that matches across the interface.

Babu et al. [Ref. 13] discussed a possible layered effect observed in the inclusions they studied (see Figure 2-9). They believe this results from the deoxidation/ desulfurization reactions and heterogeneous nucleation. Zhang and Farrar [Ref. 40] also claim inclusions act as substrates that lower the free energy barrier to nucleate acicular ferrite.

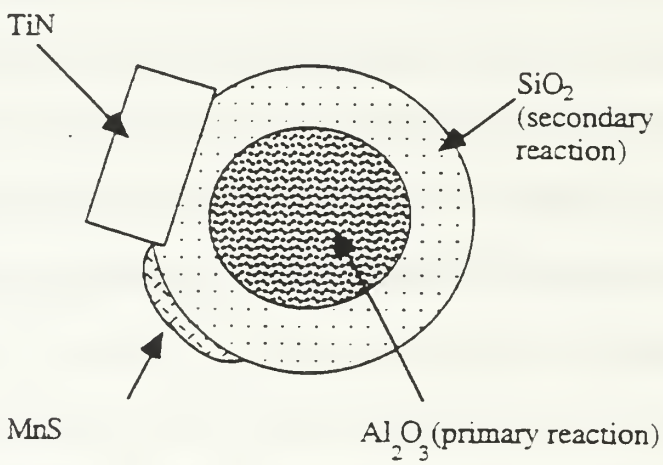


**Figure 2-9**: Schematic of a layered inclusion [From Ref. 13].

There also exists a complex reaction process of all the elements in the weld pool. Depending on the varying amounts of aluminum, titanium, sulfur, oxygen, and other elements, the resulting inclusions may or may not be strong acicular ferrite formers. Gregg and Bhadesia [Ref. 15] performed an experiment where $TiO_2$, $Ti_2O_3$, TiN, MnS, $MnO.Al_2O_3$ and $\gamma$-$Al_2O_3$ minerals in powder form were inoculated into clean melts of

molten steels. Quantitative optical microscopy measurements of isothermally transformed samples were investigated for acicular ferrite nucleation potency. Table 2-1 displays the results of the experiments.

| Mineral Addition | Area Fraction Acicular Ferrite |
|---|---|
| $MnO.Al_2O_3$ | 0.40 |
| MnS | 0.44 |
| $\gamma$-$Al_2O_3$ | 0.58 |
| TiN | 0.63 |
| $Ti_2O_3$ | 0.77 |
| $TiO_2$ | 0.91 |

**Table 2-1**. Acicular Ferrite percentage in innoculated steels [Ref. 15].

This data clearly shows that all minerals studied produced some amount of acicular ferrite in the weld metal, with the titanium oxides appearing to be the most effective. This table also shows that TiN and $\gamma$-$Al_2O_3$ are somewhat effective in nucleating acicular ferrite, while MnS and $MnO.Al_2O_3$ are less effective. Of all the minerals studied, only the titanium oxides changed in chemistry when incorporated into the melt. The titanium oxides appeared to lose oxygen in the molten steel, which coupled with the results from Table 2-1 above, led Gregg and Bhadesia to conclude the oxygen reduction reaction decarburized the steel immediately surrounding the titanium oxide, thus reducing the hardenability of the inclusion/steel matrix interface so that acicular ferrite nucleation became much easier. They surmised that it is the chemical reactions at

inclusion/matrix interfaces that is the major mechanism for accelerated acicular ferrite formation, with epitaxial growth of secondary importance although it does appear to be important since TiN and $\gamma$-$Al_2O_3$ are more effective than MnS.

Recent research [Ref. 15, 11, 38, and 40] indicates that the nucleation of acicular ferrite is an extremely complex process. There is clear evidence that many inclusions which are neither reactive chemically or have the proper orientation relationship can nucleate acicular ferrite. But they still are not as effective as inclusions that have the potential to nucleate ferrite epitaxially or those that react chemically at the inclusion/ matrix interface. Complex titanium oxides ($TiO_2$ and $Ti_2O_3$) which do not have the prerequisite lattice matching can react with the surrounding matrix through deoxidation and be reduced towards TiO, which does have good lattice matching. These results alone can help explain the strong ability of titanium-containing inclusions to nucleate acicular ferrite.

Chuen [Ref. 41] and Cochrane et al. [Ref. 36] argue that the inclusion size distribution is a major factor in promoting acicular ferrite growth. They believe fewer, larger inclusions are associated with increased levels of acicular ferrite than a higher, smaller inclusion density. Experiments have shown a build-up of carbon at the allotriomorphic ferrite/austenite interface that results from rather rapid cooling rates normally occurring in weldments [Ref. 13]. This carbon build-up inhibits the subsequent nucleation of Widmanstätten or bainite and promotes the nucleation of acicular ferrite intragranularly on larger inclusions. Inclusions too large will stunt the nucleation of acicular ferrite since deoxidation of steel to form large inclusions relies on coalescence

that would reduce the inclusion density number and thus provide fewer nucleation sites available. Coalescence also requires fairly long dwell times to form large inclusions, a luxury not normally afforded in the quick solidification rates associated with welding. There seems to be an ideal average inclusion size for the most effective acicular ferrite nucleation in steel weld metal since smaller inclusions are less effective nucleants. Indeed Zhang and Farrar [Ref. 40] assert the only reason inclusions with titanium and aluminum seem to be strong acicular ferrite formers is due to the larger average size inclusions these deoxidants generated in the weld metals studied. Unfortunately, to date no systematic measurements of acicular ferrite forming inclusion size distributions in weldments have been made.

## F. SCOPE OF PRESENT WORK

It is clear from the discussion above that the exact nature of the inclusions responsible for the nucleation of acicular ferrite is not understood. Five C-Mn steel weldments with varying amounts of deoxidizing elements (essentially aluminum and titanium), containing different volume percentages of acicular ferrite, will be studied in the present work in attempts to shed some light on the mechanisms of nucleation of acicular ferrite in ferritic steel welds.

In order to understand the role of nonmetallic inclusions in the nucleation of acicular ferrite it is necessary to consider the size, distribution, and volume fraction of the inclusions present. This will be done using the scanning electron microscope (SEM) and analyzing the final weld pass of each sample. The number of phases present and

chemistry of the inclusions present will be ascertained using carbon extraction replica samples and the transmission electron microscope (TEM) through energy dispersive x-ray (EDX) mapping and diffraction pattern analysis.

The results of this work will provide definitive size distribution data along with chemistry and crystallography information of acicular ferrite forming inclusions. Through the results of previous work and careful analysis of this data, it is hoped to discover the exact mechanisms involved in acicular ferrite nucleation and growth.

# III. EXPERIMENTAL PROCEDURE

## A. SAMPLE PRODUCTION

The five SMAW samples studied were all prepared by Dr. G. M. Evans in association with Oerlikon Welding Limited, Zurich, Switzerland. Essentially these five samples were chosen as the only major difference from sample to sample is the amount of aluminum and titanium composition within the weld. The complete weld sample preparation is included in Reference 8. The following is a quick overview:

### 1. Electrodes

Different amounts of aluminum and titanium were added to the coatings of five basic low hydrogen electrodes to obtain weld samples with varying deoxidizer levels. The electrodes were then extruded onto 4 mm core wire to bring the coating to electrode diameter ratio (D/d) to 1.68 inches. Table 3-1 displays the final weld metal Al and Ti compositions of the five samples studied.

| SAMPLE | ALUMINUM | TITANIUM |
|---|---|---|
| | ppm | |
| O | 6 | 1 |
| W | 5 | 28 |
| Y | 13 | 390 |
| Z | 160 | 420 |
| V | 580 | 540 |

**Table 3-1**. Coatings of Sample Electrodes.

### 2. Weld Preparation

The joint geometry is specified in ISO 2560-1973. Welding was done in the flat position with three beads per layer until 27 total number of runs were deposited. The welding parameters used: 170 A in direct current, 21 volts voltage, 1 kJ/mm heat-input, and a 200 °C interpass temperature maintained.

### 3. Heat-Treatment

All weld samples were tested in the "as-deposited" condition. Samples were given a 14 hour 250 °C hydrogen removal heat treatment and a 2 hour 580 °C heat treatment for tensile and stress relieved toughness tests respectively.

### 4. Mechanical Testing

Two all-weld metal samples were cut from each weldment, and approximately 35 Charpy-V notch specimens were tested for each weldment. This provided a full transition curve for each weldment.

### 5. Metallography

Transverse sections of each weldment were prepared and analyzed optically. This detailed optical examination was performed on the top three beads and on the adjacent reheated zones. This area will be called the last weld pass.

## 6. Summary

Dr. Evans [Ref. 8] provided chemical composition and mechanical properties of all five samples. The five weldments were prepared in a controlled environmental condition to ensure desired compositions. Table 3-2 displays the chemical compositions of the five samples studied in the present work.

| | C | Mn | Si | S | P | Ti | B | Al | N | O |
|---|---|---|---|---|---|---|---|---|---|---|
| | % | | | | | ppm | | | | |
| O | 0.074 | 1.4 | 0.25 | 0.008 | 0.007 | 1 | 1 | 6 | 79 | 475 |
| W | 0.077 | 1.46 | 0.27 | 0.008 | 0.007 | 28 | 3 | 5 | 81 | 459 |
| Y | 0.070 | 1.57 | 0.45 | 0.006 | 0.010 | 390 | 39 | 13 | 83 | 308 |
| Z | 0.072 | 1.56 | 0.49 | 0.007 | 0.010 | 420 | 48 | 160 | 67 | 438 |
| V | 0.078 | 1.44 | 0.60 | 0.006 | 0.007 | 540 | 56 | 580 | 41 | 336 |

**Table 3-2**. Chemical Composition of five samples [From Ref. 8].

The mechanical properties listed in Table 3-3 contain information on the "as-welded" properties as previously discussed. Shelf temperatures of 100J and 28J Charpy-V notch tests are also included in the table.

| | YS | EL | RA | ISO-V | |
|---|---|---|---|---|---|
| | MPA | % | % | 100J | 28J |
| O | 445 | 28.2 | 78.0 | -14 | -42 |
| W | 471 | 25.2 | 77.0 | -68 | -88 |
| Y | 546 | 25.8 | 73.0 | -84 | -114 |
| Z | 610 | 27.2 | 73.4 | -83 | -100 |
| V | 668 | 20.2 | 69.4 | -12 | -46 |

**Table 3-3**. Mechanical Properties of five samples studied [Ref. 8].

## B. SAMPLE PREPARATION

The five weld samples were cut into one inch transverse pieces for analysis. Each specimen was ground and polished progressing through the following process: (i) grinding on 180, 320, 500 and 1000 grit Struers and Buehler silicon carbon paper, (ii) polishing using 3μm followed by 1μm diamond compound on Buehler Microcloth.

## C. OPTICAL MICROSCOPY

To reveal the weld deposit microstructure, a twenty second etch using 5% nital (5% nitric acid and 95% methanol) was performed on all weld samples. This light etch allowed the use of optical microscopy to actually see the acicular ferrite morphology and other microconstituents. Various micrographs were then taken of each sample in the fusion zone, where the long columnar grains exist, and the reaustenitized zone, where fine equiaxed grains were produced. The average prior austenite grain width was measured in the columnar grain region to compare from sample to sample. Micrographs were taken on a Zeiss Jenaphot 2000 optical photomicroscope with an attached Pulnix TMC-74 optical camera. This camera was connected to a 486/DX2 computer equipped with Semicap photo analysis software to produce the digital photographs.

## D. SCANNING ELECTRON MICROSCOPY (SEM)

### 1. Objective

SEM analysis provides critical information on the average inclusion size, distribution and volume fraction. The average inclusion size, distribution and volume fraction data for each sample were compared to see how these affect acicular ferrite nucleation.

### 2. SEM Overview

The basic function of a Scanning Electron Microscope (SEM) is to produce a three dimensional appearing image derived from the action of an electron beam scanning across the surface of the specimen. The size and shape of features on the specimen's surface can be examined, as can features just below the surface depending on the type of imaging electrons used. Figure 3-1 displays a schematic of a typical SEM.

The SEM consists of five major parts: (i) the *Electron Gun* emits a large high-intensity electron beam down the column, (ii) the *Column* controls and focuses the electron beam into a size useful for scanning microscopy (~ 100nm), (iii) the *Scanning System* scans the beam over the specimen in a pattern which is called a raster, (iv) the *Electron Collector and Display* collects emitted electrons and converts them to a viewable image, and (v) the *Control Electronics* controls all the above.

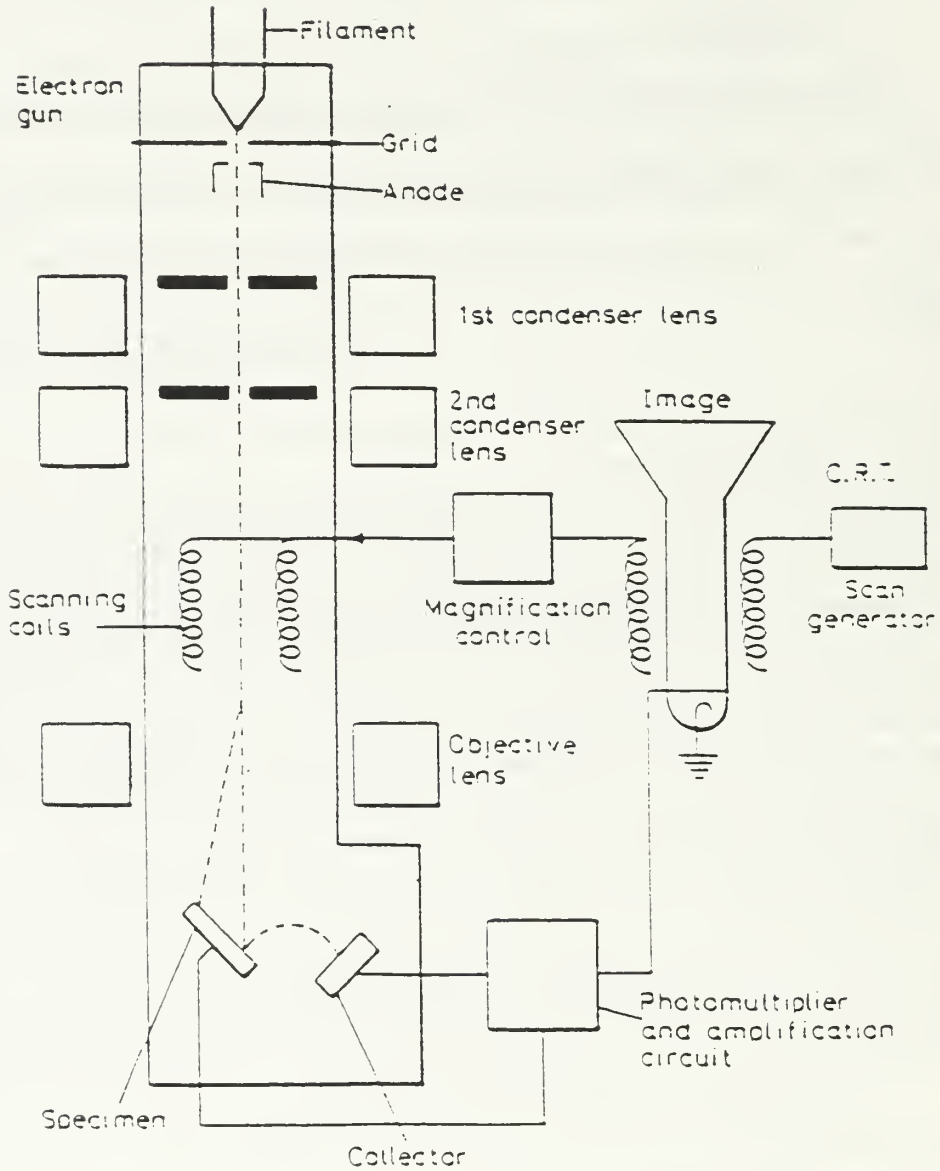


**Figure 3-1**. Schematic of a typical scanning electron microscope (SEM).

When the electrons strike the surface of the sample, interactions occur within the material. These interactions lead to the emission of backscattered electrons, secondary electrons, Auger electrons and X-rays that can be used to generate images or chemical information of the sample. Figure 3-2 displays the signals produced by a typical scanning electron microscope. Light is also produced, but a special cathodoluminesence detector is needed to see it.

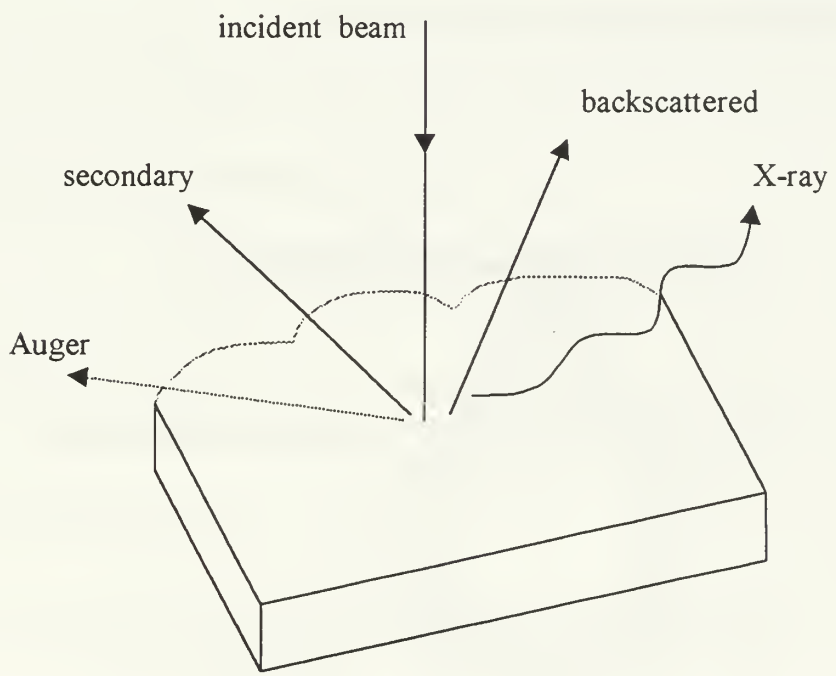


**Figure 3-2**. Sketch of signals produced by a typical SEM.

### 3. Procedure

The present work used secondary electron imaging as opposed to backscattered electron produced images. Kluken et al. [Ref. 44] discussed the possible problem of underlying inclusions being counted as surface inclusions when using backscattered electron images. This is due to the nature of how deep into the specimen the interactions take place for the given imaging process. Using the assumption that area fraction and volume fraction are similar for surface inclusions, the decision to use secondary electron imaging was made. Figure 3-3 displays a sketch of the possible depths of emitted electrons produced from a scanning electron microscope.

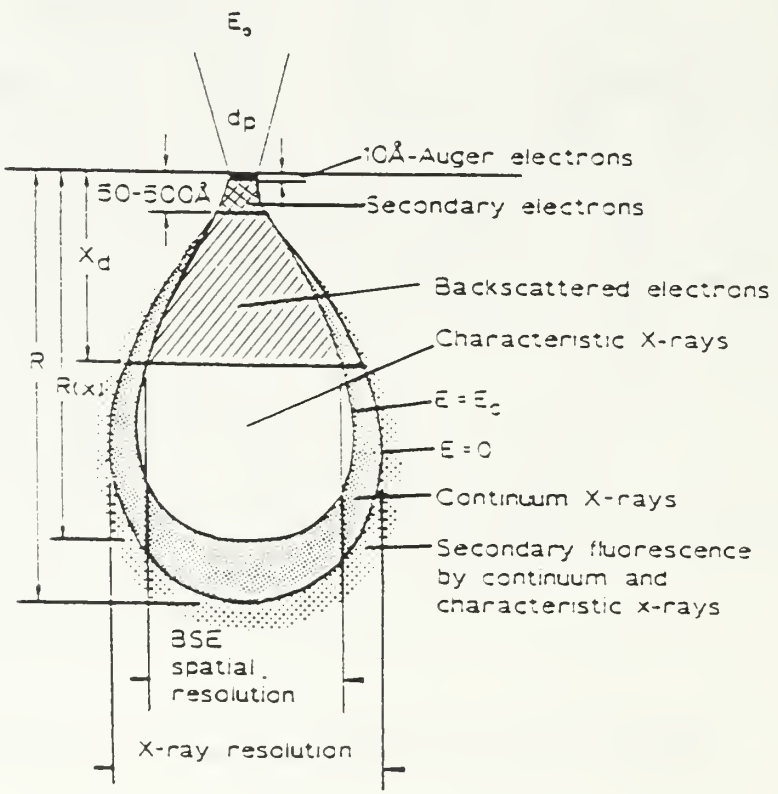


**Figure 3-3**. Sketch of possible depths of various emitted electrons from a SEM.

The Topcon SM-510 Scanning Electron Microscope was used to obtain inclusion size distribution data. This SEM is connected to a 486/DX2 computer equipped with Link ISIS and Link Tetra software. Using 20kV accelerating voltage, 5000X magnification and a 10mm working distance, one hundred secondary electron images were taken for each sample. The secondary electron image resulted in micrographs with good contrast and high resolution for inclusion counting and sizing. Only inclusions greater than 0.15 micron in diameter were recorded. These micrographs also had a micron marker inscribed on them, which made the total area studied calculations simple (411.67 μm). A mean value of the number of inclusions per field and diameter were calculated with a 95% confidence interval. The volume fraction was then calculated for each weld sample using the following equation:

$$\text{Volume Fraction} = (s\pi d^2) / (4f) \qquad 3.1$$

where

s = average number of inclusions per field  d = mean diameter of inclusions

f = inclusion field size

The 95% confidence interval was calculated using the following formula:

$$CI = +/- 1.96 (\sigma/\text{sqrt}(n)) \qquad 3.2$$

where

n = population  $\sigma$ = standard deviation $\Rightarrow [(n\Sigma x^2-(\Sigma x)^2) / (n(n-1)]^{1/2}$ 3.3

where x = the range on either side of the sample mean that 95% of all the data lay.

## E. TRANSMISSION ELECTRON MICROSCOPY (TEM)

### 1. Objective

The transmission electron microscope (TEM) is one of the most effective tools to analyze the morphology, crystal structure and chemical composition of nonmetallic inclusions. The present work uses carbon extraction replicas and the TEM in conjunction with energy dispersive x-ray spectroscopy (EDX), EDX mapping and diffraction pattern analysis to investigate and determine the exact nature of the phases present on the acicular ferrite-forming inclusions. It should be mentioned here that inclusions size determinations are not normally done using the TEM because it is difficult to get enough fields for analysis, although further work could use carbon extraction replicas and the TEM to study size and chemistry and possibly investigate chemistry as a function of size.

### 2. TEM Overview

Like the SEM, the TEM uses electron interactions to produce imaging and chemical information. The difference between the TEM and SEM is the high spatial resolution provided by the TEM. The present work used the TOPCON 002B TEM with a $LaB_6$ crystal energized to 200,000 volts, accelerating the electrons at the carbon extraction replica samples to a very short wavelength. This provides a spatial resolution in imaging of approximately 0.18nm. EDX analysis was performed using a smallest electron probe diameter of 5nm.

The TEM consists of an electron gun and a series of magnetic condenser lenses that are enclosed in an evacuated column. The electron source ($LaB_6$ crystal in the present work) emits the electrons that are then accelerated by the electron gun down the column. The condenser lenses collimate the electron beam at the sample (carbon extraction replica of inclusions in present work). The electrons continue through the sample and produce a sample image that is magnified by additional lenses and projected onto a fluorescent screen. By removing the optical aperture and inserting a selected-area diffraction aperture, diffraction patterns are produced. Figure 3-4 displays a sketch of a typical TEM and how imaging or diffraction patterns can be generated.

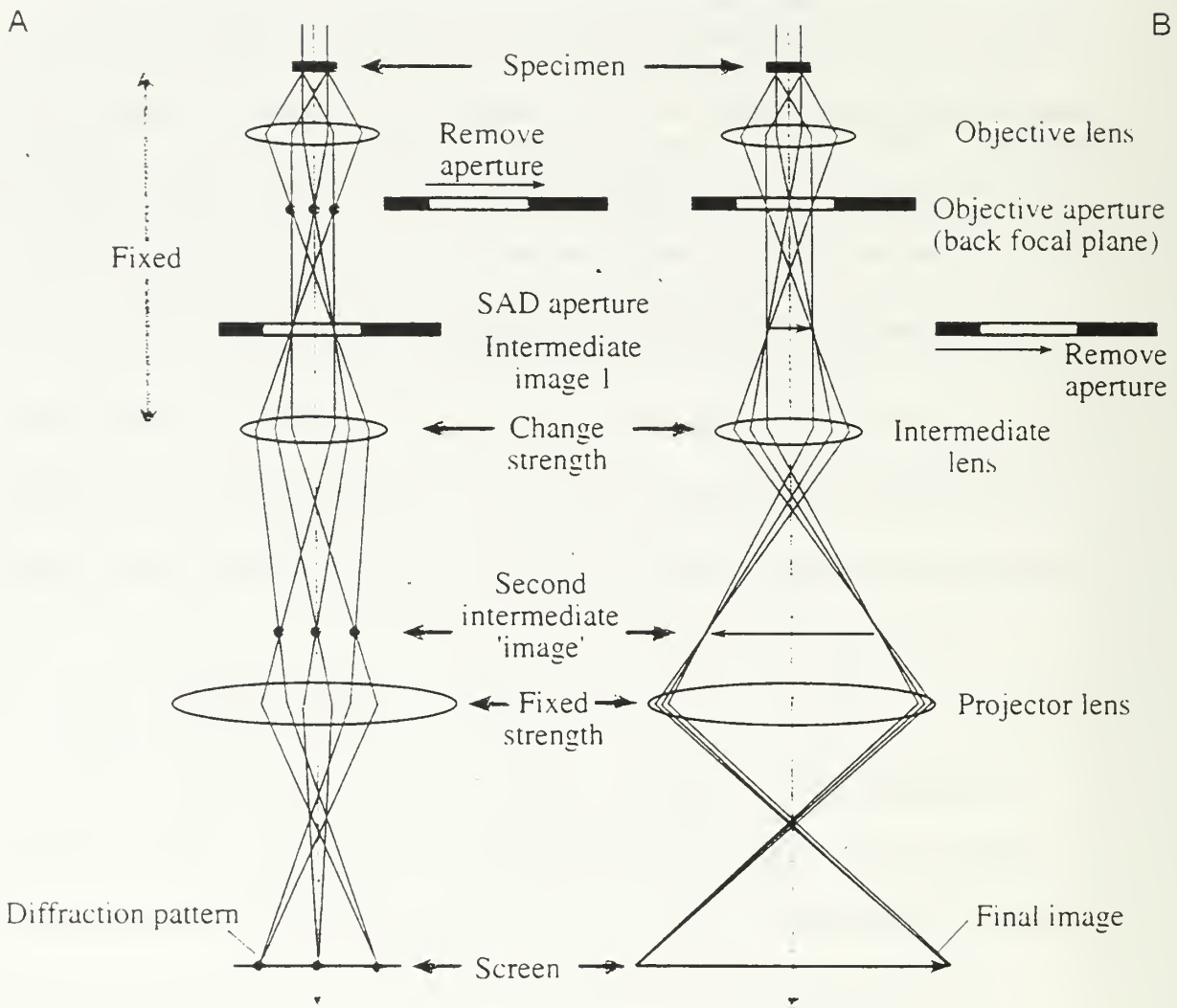


**Figure 3-4**. Schematic of TEM projecting (a) diffraction patterns and (b) imaging onto a fluorescent screen [From Ref. 45].

### 3. Carbon Extraction Replicas

Carbon extraction replicas of the five weld sample inclusions were produced for TEM study. The five weld samples were repolished and lightly etch in 5% nital for twenty seconds. This exposed the nonmetallic inclusions on the surface of the weld sample. The samples were then masked such that only the last weld pass was revealed. Samples were then placed into a vacuum chamber of a Ernest F. Fullan Mk II carbon coater. Two carbon strands were wound together and placed between electrodes at a distance of 3.1 cm above the sample. After the chamber was evacuated, a current was passed through the carbon strands depositing a fine layer of carbon on the exposed portion of the sample. This process was repeated until a bluish-gold film appeared representing a film thickness of approximately 20nm. Three milimeter squares were then scribed on the coated sample area and the masking material removed. The sample was then placed in a bath of 5% nital for extended etching. After approximately five minutes the coating squares began to float off of the sample. These carbon extraction replicas, containing the nonmetallic inclusions from the weld sample, were then gently lifted from the nital solution and placed into a 5% acetone bath. The acetone bath flattened the replicas due to surface tension effects and made it easier to remove the replicas with 400 mesh nickel grids. Nickel grids were chosen over copper grids due to the presence of a copper sulfide phase on the inclusions being detected by the TEM.

### 4. Energy Dispersive X-ray (EDX) Spectroscopy

The x-rays that were emitted from the inclusions in the replicas were detected using an energy dispersive x-ray (EDX) detector. The TEM electron beam interacts with the carbon extraction replica inclusion atoms and ionize an inner shell electron which causes an outer shell electron to reduce its energy and fill this inner shell vacancy. This causes characteristic x-rays to be emitted and these contain energy information. Measurement of these x-ray energies is performed with a lithium drifted silicon, (SiLi), detector. Each x-ray has a certain amount of energy depending on the distance from the nucleus to the outer shell used to fill the missing electron position. The energy of the x-ray is quanitized resulting in each element having its own characteristic x-ray spectrum. Figure 3-5 displays a sketch of the EDX capture process.

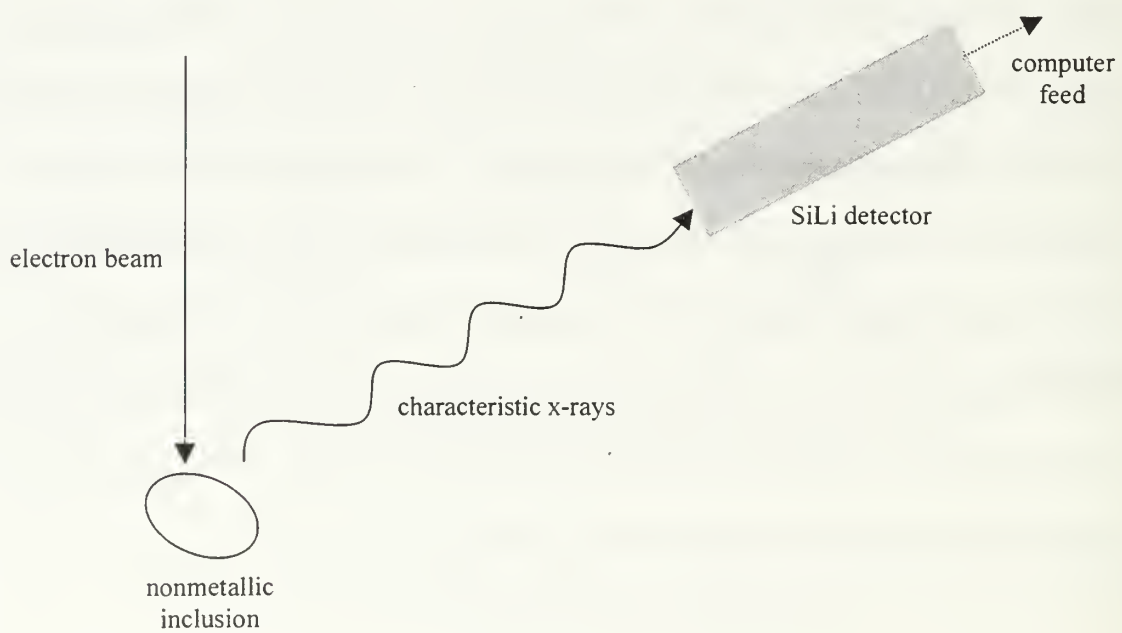


**Figure 3-5**. Sketch of EDX detector arrangement.

The way these characteristic x-rays are quanitized is through the use of an energy dispersive x-ray spectrometer. The x-rays pass through the SiLi detector which generates voltage pulses the number of which is proportional to the x-ray energy. These pulses are input into a pulse processor and a multi channel analyzer to produce an intensity (or counts) versus x-ray energy response. This information is graphically portrayed as intensity versus energy in an EDX spectrum. From this spectrum a quantitative and qualitative assessment of the elements present in the inclusion may be deduced from each elements' characteristic energy lines. A typical EDX spectrum is portrayed in Figure 3-6.

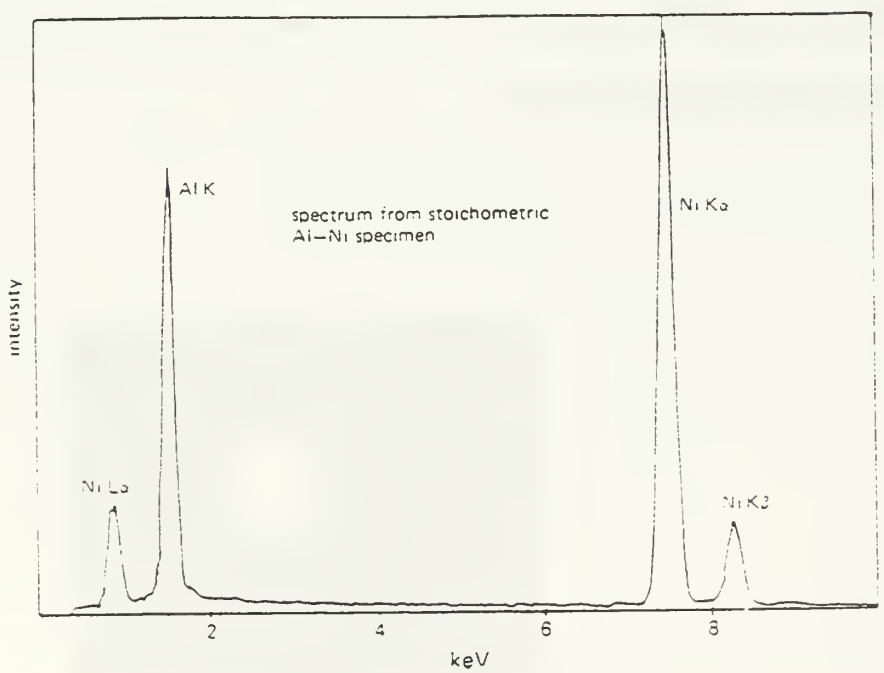


**Figure 3-6**. Typical EDX spectrum.

### 5. Diffraction

Conventional electron diffraction patterns are created from the Bragg diffraction of elastically scattered electrons. As the electron beam passes through the carbon extraction replica, a portion of the electron beam is scattered at small angles producing spot diffraction patterns. The pattern from a single inclusion region represents a set of planes that belong to the same crystallographic zone. The measurement of the angle of diffraction and the wavelength of the electrons being diffracted allows a calculation of the distance between planes of atoms in the inclusion. These distances provide the means to determine the Bravais lattice of the inclusion crystal structure. This information coupled with EDX data can lead to the complete characterization of the phases in the inclusions. Unfortunately the inclusions that nucleate acicular ferrite are usually multiphase and polycrystalline which makes the analysis difficult. Figure 3-7 displays a typical inclusion diffraction pattern.

**Figure 3-7**. Typical inclusion diffraction pattern.

## 6. Summary

Optical Microscopy was used in the present work to measure and compare the average prior austenite grain widths for each sample. Scanning electron microscopy enables the average inclusion size, distribution and volume fraction to be determined. Transmission electron microscopy is used to determine inclusion crystal structures and chemical composition by EDX and diffraction pattern analysis of carbon extraction replicas. These techniques together should unlock many of the mysteries surrounding the mechanisms of nucleation of acicular ferrite in steel welds.

# IV. RESULTS AND ANALYSIS

## A. WELD COMPOSITION

As previously presented, the chemical compositions of the five samples were provided by Dr. G. M. Evans. All alloying elements were held fairly constant except for varying amounts of titanium and aluminum. Table 4-1 is the chemical composition of the five samples studied. Typical errors in the chemical analysis of these elements are Mn - 0.02; Si - 0.01; Al and P - 0.002; C, S, Ti, O, N and B - 0.001 (wt %).

| | C | Mn | Si | S | P | Ti | B | Al | N | O |
|---|---|---|---|---|---|---|---|---|---|---|
| | % | | | | | ppm | | | | |
| O | 0.074 | 1.4 | 0.25 | 0.008 | 0.007 | 1 | 1 | 6 | 79 | 475 |
| W | 0.077 | 1.46 | 0.27 | 0.008 | 0.007 | 28 | 3 | 5 | 81 | 459 |
| Y | 0.070 | 1.57 | 0.45 | 0.006 | 0.010 | 390 | 39 | 13 | 83 | 308 |
| Z | 0.072 | 1.56 | 0.49 | 0.007 | 0.010 | 420 | 48 | 160 | 67 | 438 |
| V | 0.078 | 1.44 | 0.60 | 0.006 | 0.007 | 540 | 56 | 580 | 41 | 336 |

**Table 4-1**. Chemical Composition of five samples (wt %) [From Ref. 8].

## B. OPTICAL MICROSCOPY

The average prior austenite grain sizes for the five samples were measured in the fusion zone where the long columnar grains exist. Each sample had varying amounts of acicular ferrite and other microconstituents revealed by the light nital etch. Of all the microstructures, Sample O has the lowest amount of acicular ferrite present and Sample W has enough to be representative of the other three samples. Figure 4-1 and Figure 4-2 are optical micrographs of the final weld pass of sample O and sample W at low magnification. Notice the long columnar grains.

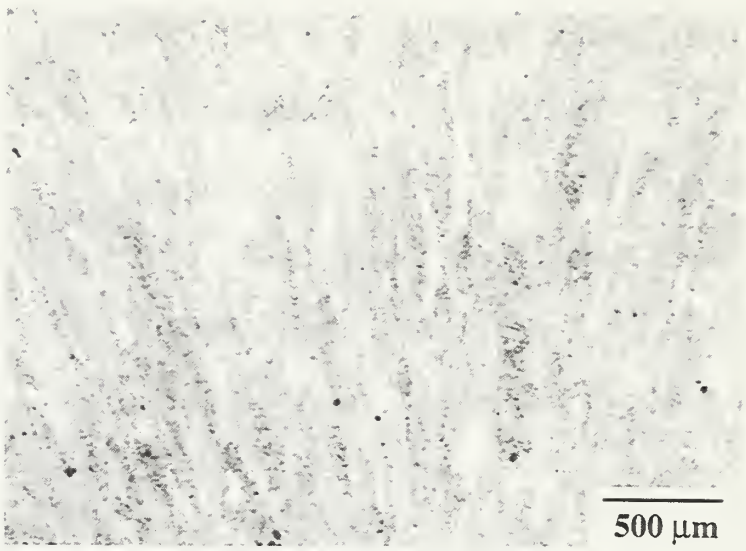


**Figure 4-1**. Optical micrograph of final weld pass for Sample O.

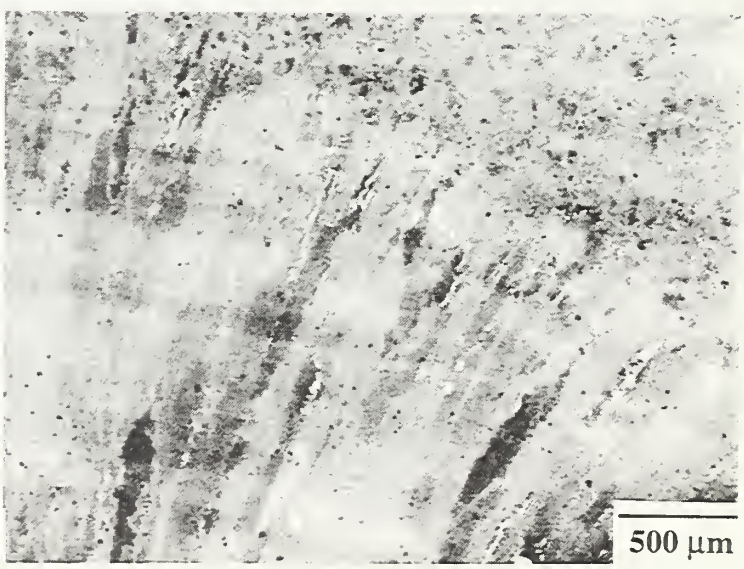


**Figure 4-2**. Optical micrograph of final weld pass for Sample W.

The average prior austenite grain size was calculated using multiple micrographs similar to Figure 4-3 and Figure 4-4. Again these figures only display a micrograph from sample O and the "representative" sample W. Calculation of the average prior austenite grain boundary was 100μm +/- 25μm for all five samples. This calculation shows how the average prior austenite grain size does not change significantly from sample to sample regardless of the amount of acicular ferrite obtained within the microstructure.

The reaustenitized grains between weld passes were equiaxed. The grain size in this area also did not change significantly from sample to sample except for sample O. The morphology was quite different, as sample O does not have appreciable amounts of acicular ferrite in the weld metal and Widmanstätten ferrite and bainite dominate the microstructure. When acicular ferrite is reaustenitized, a smaller grain size is produced. These reaustenitized grains are apparently much smaller than reaustenitized regions in sample O which has only small amounts of acicular ferrite in the as-deposited condition. Consequently, the reaustenitized regions of samples containing large amounts of acicular ferrite are likely to have a lower hardenability than sample O. As a result, samples containing appreciable levels of acicular ferrite transform to small, tough, equiaxed, ferrite grains where as reaustenitized regions of sample O transform to larger grained mixtures of ferrite and bainite. Figure 4-5 and Figure 4-6 are micrographs of the reaustenitized region of sample O and sample W. Note the morphology and size of grains.

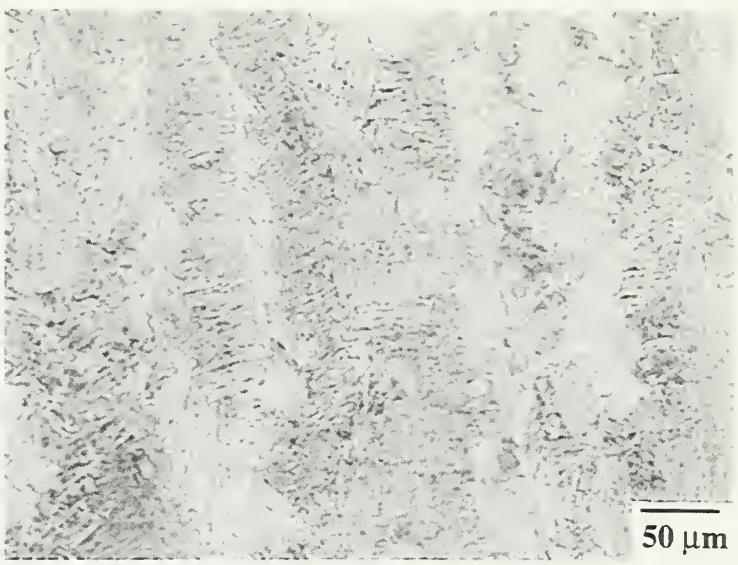


**Figure 4-3**. Optical micrograph of final weld pass for Sample O.

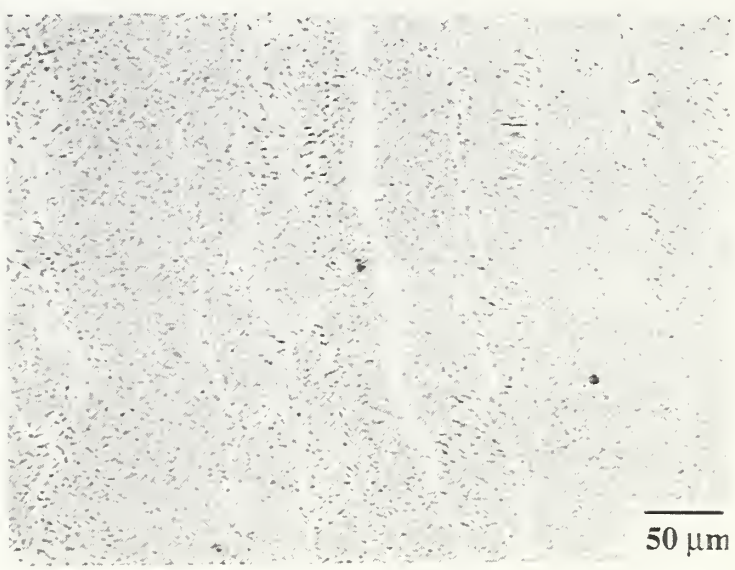


**Figure 4-4**. Optical micrograph of final weld pass for Sample W.

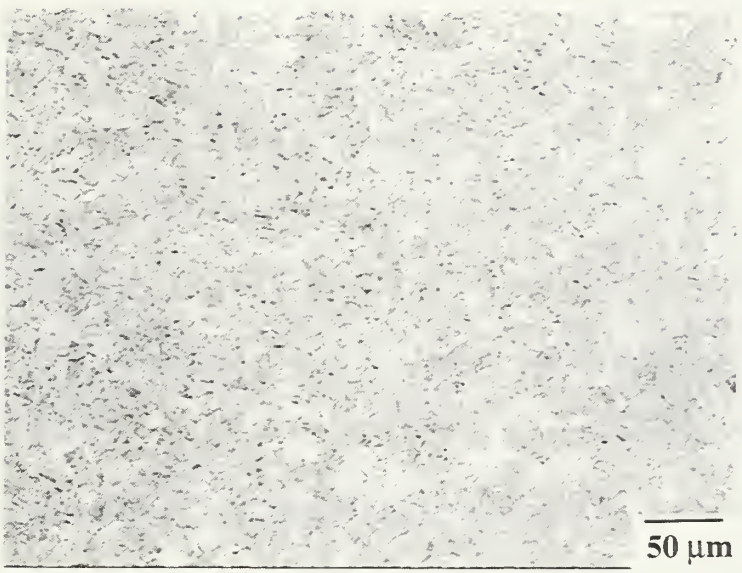


**Figure 4-5**. Optical micrograph of reaustenitized region for Sample O.

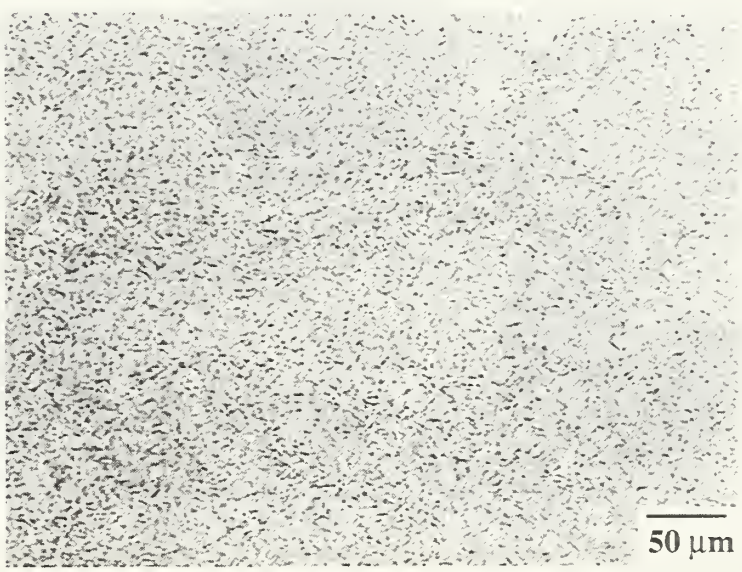


**Figure 4-6**. Optical micrograph of reaustenitized region for Sample W.

## C. ACICULAR FERRITE IN WELD METAL

Dr. G. M. Evans used optical examination of the last pass weld bead to determine and quantify the major microstructural components within each weld sample [Ref. 8]. Reference 3 was used to identify the microstructure through the use of a manual point count survey. The results show what was expected of the microstructure. Sample O has the lowest level of acicular ferrite at 12% and the other four samples run between 65 – 92 % acicular ferrite. The remaining phases were primary ferrite and ferrite with second phase. Figures 4-7 and 4-8 show graphically the amounts of major microstructural components in each of the weld samples studied.

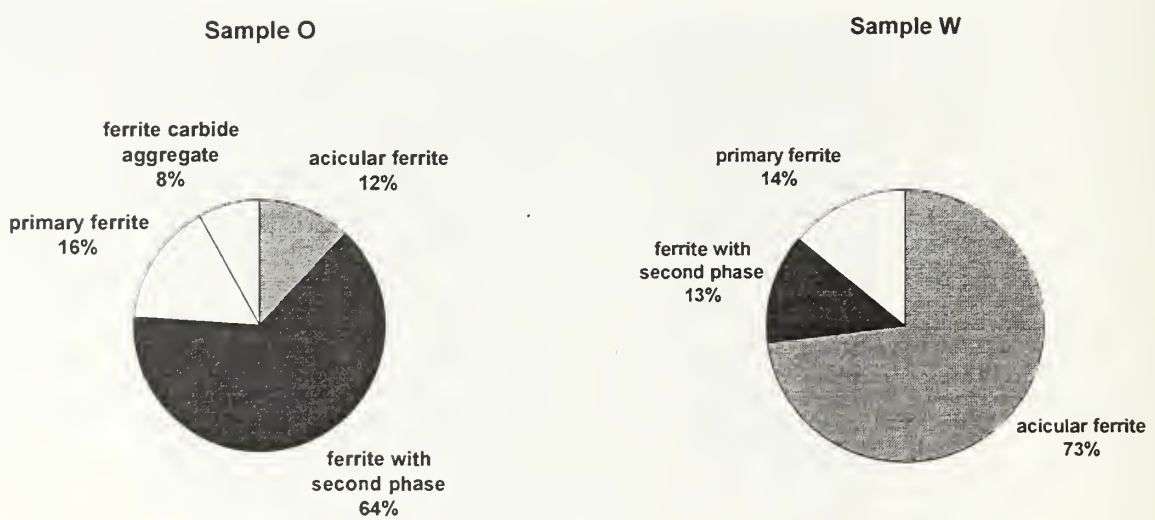


**Figure 4-7.** Pie charts of microconstituents in Sample O and Sample W.

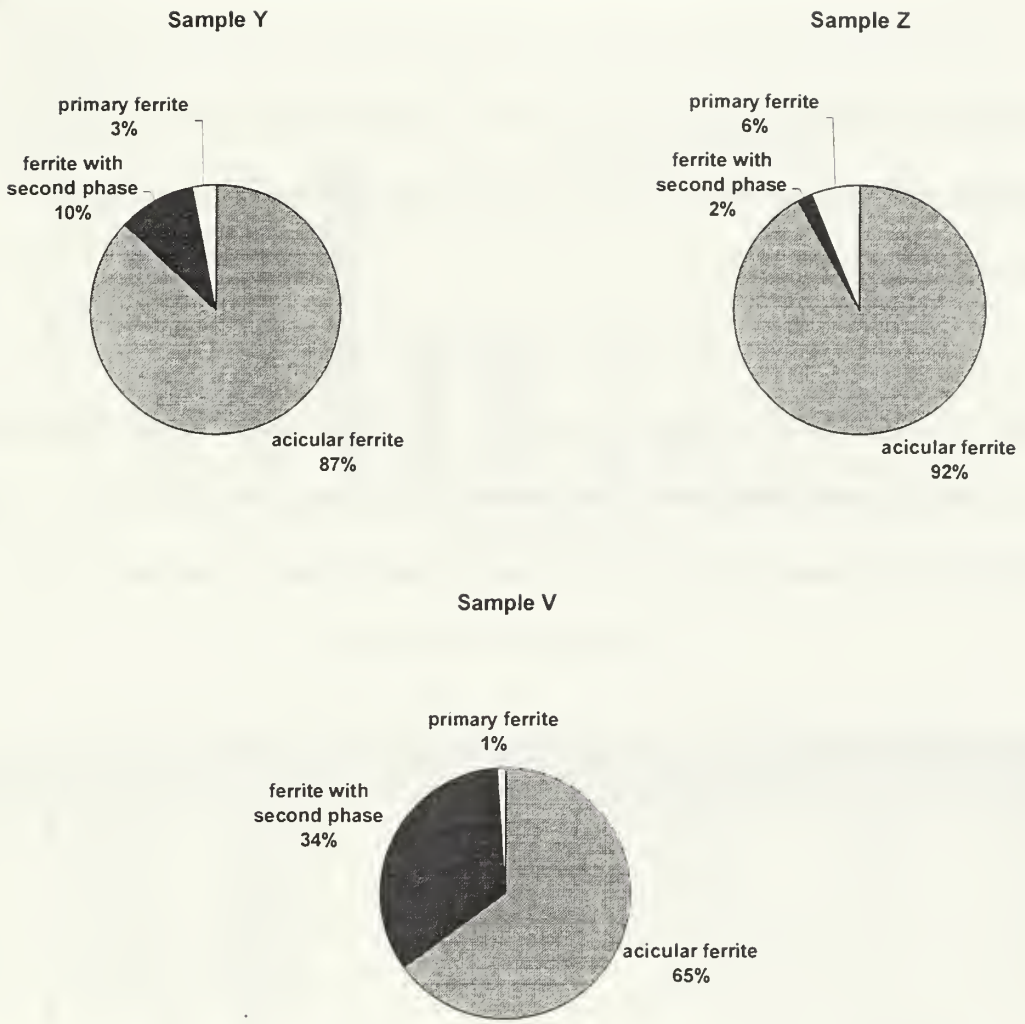


**Figure 4-8**. Pie charts of microstructure for Sample Y, Z, and V

All things being equal, it seems from these pie charts, that the samples with a higher ratio of titanium to aluminum are stronger acicular ferrite formers.

## D. INCLUSION SIZE DISTRIBUTION AND VOLUME FRACTION

The average size and number of inclusions for each sample were measured using the SEM as described in the last section. The volume fractions were also calculated and compared with theoretical results [Ref. 51] for Si-Mn deoxidants only using the following equation:

$$V_f \approx 0.05w_o + 0.054(w_s - w_s^{sol}) \qquad 4.1$$

where, $w_o$ represents the concentration of the element in units of weight percent and $w_s^{sol}$ is the soluable sulphur concentration (usually assumed to be 0.003 wt%). Table 4-2 shows the inclusion size and volume fraction data for the five samples studied.

| sample | # inclusions | Mean size (μm) +/- CI* | % AF | $V_f$ (avg) | $V_f$ (theory) |
|---|---|---|---|---|---|
| O | 1635 | 0.3033 +/- .02311 | 12 | 0.00287 +/- .00043 | 0.002645 |
| W | 1339 | 0.2405 +/- .01713 | 73 | 0.00148 +/- .00021 | 0.002565 |
| Y | 639 | 0.2047 +/- .01145 | 87 | 0.00051 +/- .00006 | 0.001702 |
| Z | 775 | 0.2154 +/- .01388 | 92 | 0.00069 +/- .00009 | 0.002400 |
| V | 630 | 0.2406 +/- .01691 | 65 | 0.00071 +/- .00010 | 0.001842 |

* 95% Confidence Interval

**Table 4-2.** Average Inclusion Size and Volume Fraction for Samples O through V.

The inclusion size distributions were analyzed and are presented in Figures 4-9 through 4-11. The average inclusion size varied from sample to sample. The distributions all seemed to follow a similar pattern with anything less than 0.15μm not measured in the SEM.

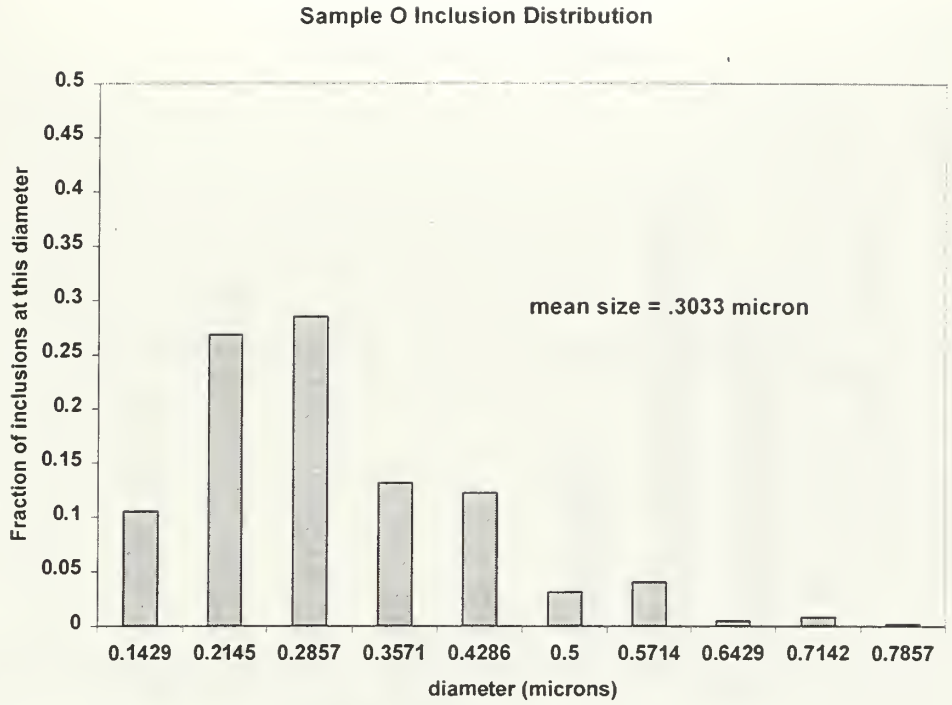


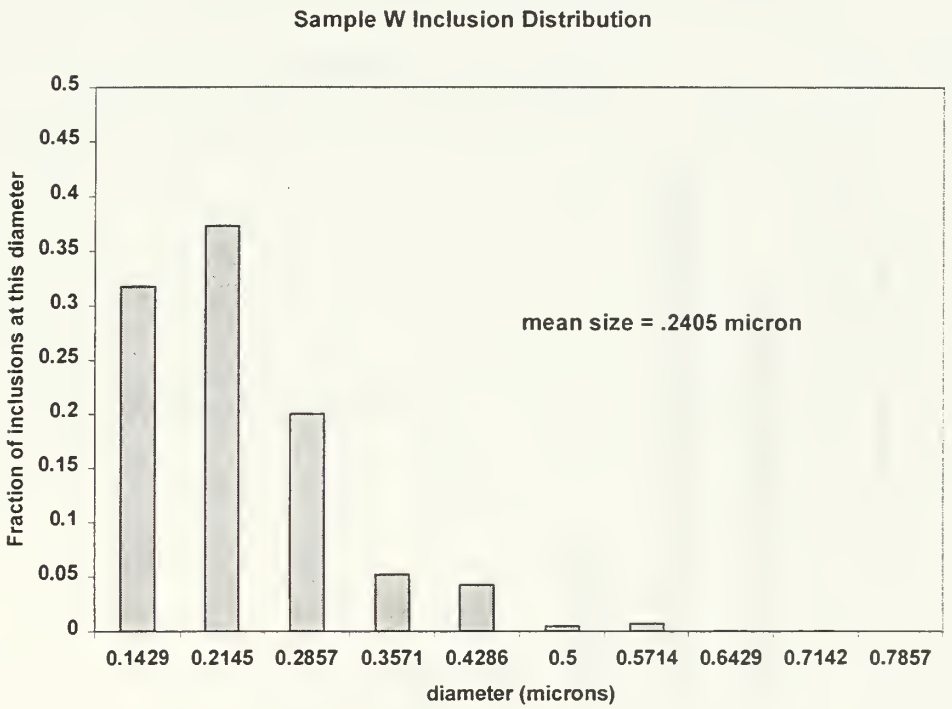


**Figure 4-9**. Inclusion Distribution for Sample O and Sample W.

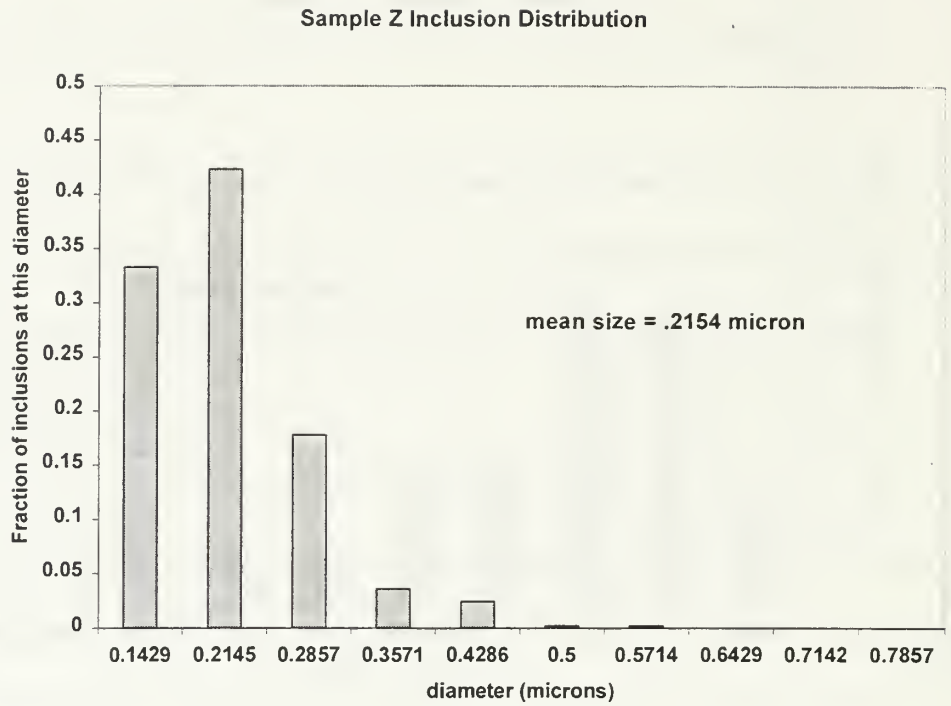


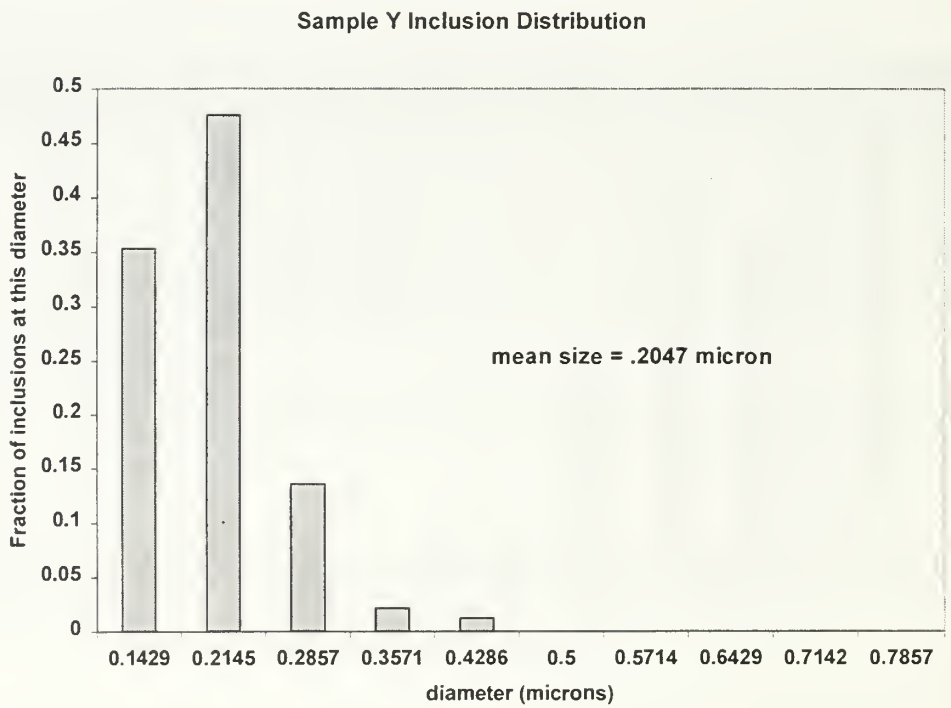


**Figure 4-10**. Inclusion Distribution for Sample Y and Sample Z.

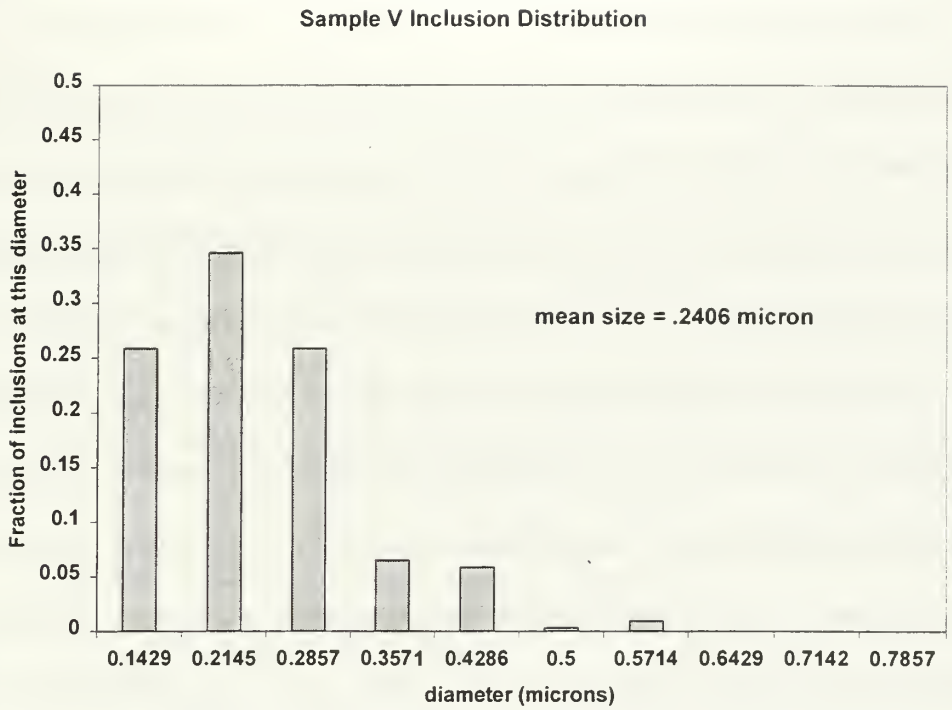


**Figure 4-11**. Inclusion Distribution for Sample V.

Using the data tabulated in Table 4-2, investigations can be made to see if these results corroborate previous work and presently accepted theory on the mechanisms of acicular ferrite nucleation. First a plot of the volume fraction versus amount of oxygen present in each sample's weld metal is produced. Theory [Ref. 46] suggests when only silicon and manganese are present as deoxidants, the ratio of volume fraction to oxygen content should follow a straight line. Indeed Sample O, with only 1ppm titanium and 6 ppm aluminum, falls very close to this theoretical straight line depicted in Figure 4-12. Deviations from theory result when increasing levels of aluminum and titanium are added to the weld metal composition. With the addition of even small amounts of these strong deoxidants, as in Sample W with 28 ppm Ti and 5 ppm Al, the volume fraction of inclusions decreases rapidly, to a point where given appreciable levels of Ti and Al, the volume fraction appears to be constant regardless of oxygen content.

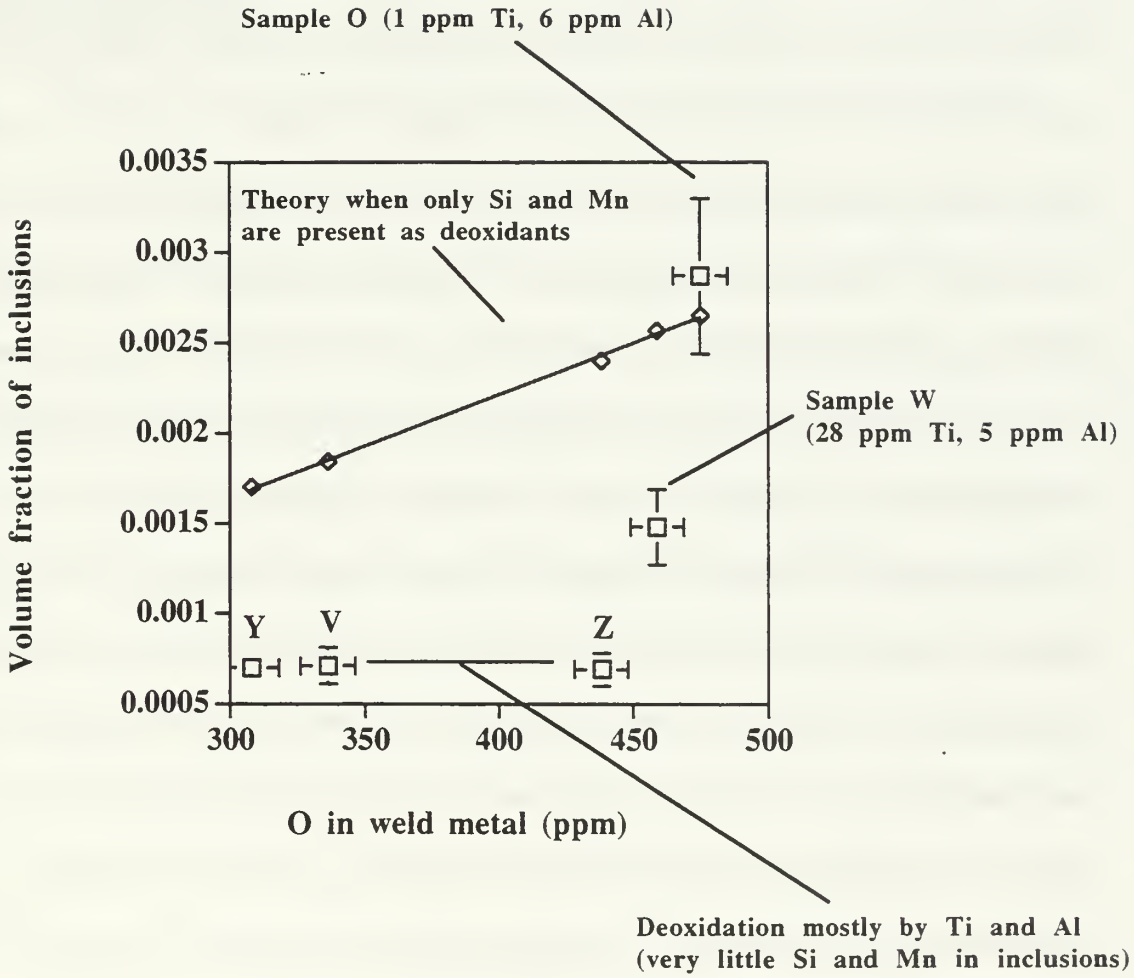


**Figure 4-12**. Inclusion volume fraction vs. weld metal oxygen.

Before discussing these results further, some previous work will now be presented and used for comparison. Greene [Ref. 50] and Walters [Ref. 39] made preliminary TEM/EDX investigations into the five samples studied in the present work. Table 4-3 displays this information in tabular form. Their work gives a good synopsis of the inclusions' elemental compositions for a given sample. The results are briefly outlined here. Sample O, containing very little Ti and Al, weld metal contains inclusions dominated by the oxide $MnO.SiO_2$, which does not seem to be a strong acicular ferrite former since only 12% is present in the weld. Sample W, 28 ppm Ti and 3 ppm Al, has a higher level of Ti added resulting in titanium-containing oxide(s) present in the inclusions as well as the $MnO.SiO_2$ as previously seen. The greater amounts of Ti seem to help in nucleating acicular ferrite as the volume percent reaches 75% in the weld metal. Sample Y, 390 ppm Ti and 13 ppm Al, has much higher levels of Ti than Al in the weld metal resulting in inclusions dominated by titanium-containing oxides and acicular ferrite content increases to 87 volume %. Sample Z, 420 ppm Ti and 160 ppm Al, has more Al added to the weld which results in inclusions that appear to have a mixture of a titanium oxide(s) and $Al_2O_3$ with acicular ferrite jumping to 92 volume %. Finally Sample V, 540 ppm Ti and 580 ppm Al, with nearly equal amounts of Ti and Al has inclusions that appear to be complexes of TiN, titanium oxide(s) and $Al_2O_3$ with acicular ferrite content of 65 volume %. The researchers mentioned earlier also provided data on the atomic percent of aluminum and titanium found in the inclusions of each sample. It should also be pointed out here that Parallel Electron Energy Loss Spectroscopy (PEELS) work by

Walters [Ref. 39] suggested that the Ti was present as TiO except for sample V where some TiN was also detected.

| Sample | % Acicular Ferrite | Atomic % Ti | Atomic % Al |
|---|---|---|---|
| O | 12 | 0 | 0 |
| W | 73 | 7 +/- 4 | 0 |
| Y | 87 | 75.79 +/- 11.77 | 2.09 +/- 1.60 |
| Z | 92 | 45.17 +/- 13.23 | 41.85 +/- 11.52 |
| V | 65 | 29.16 +/- 9.62 | 57.82 +/- 10.18 |

**Table 4-3**. Average atomic % of titanium and aluminum found in inclusions.

The next investigation was to investigate the effects of varying aluminum and titanium in the weld metal. Starting with aluminum and looking purely at the volume percent of acicular ferrite vs. the amount (ppm) of aluminum in the weld metal (Figure 4-13), gives us an interesting picture of why aluminum-containing oxides have been thought to be strong acicular ferrite formers. Notice from Figure 4-13, however, that adding too much aluminum seems to have a deleterious effect on the acicular ferrite content of the final weld metal microstructure. The best way to look at how aluminum content effects acicular ferrite nucleation is to plot the volume percent of acicular ferrite vs. the *atomic percent* of aluminum in the inclusions (Figure 4-14). This graph clearly shows that, although aluminum seems to be a strong acicular ferrite former, something else seems to be the driving force for obtaining high levels of acicular ferrite in the weld metal. This is supported by the work of Evans and Bailey [Ref. 52] who showed that weld metals similar to those shown in Table 4-1 which were deoxidized with aluminum only (no Ti) contained low levels of acicular ferrite (~ 21 vol. % max).

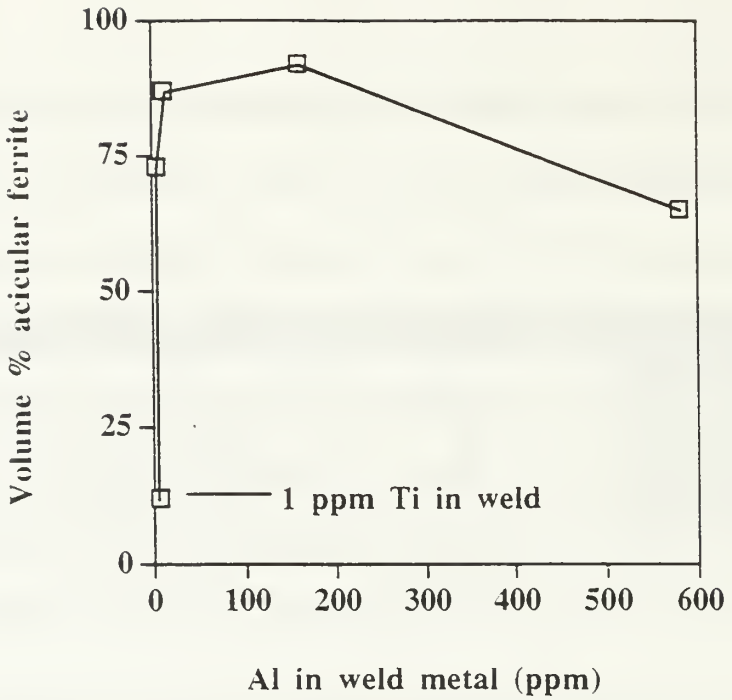


**Figure 4-13**. Volume percent acicular ferrite vs. weld metal aluminum. (The errors for both axes are less than the symbol size)

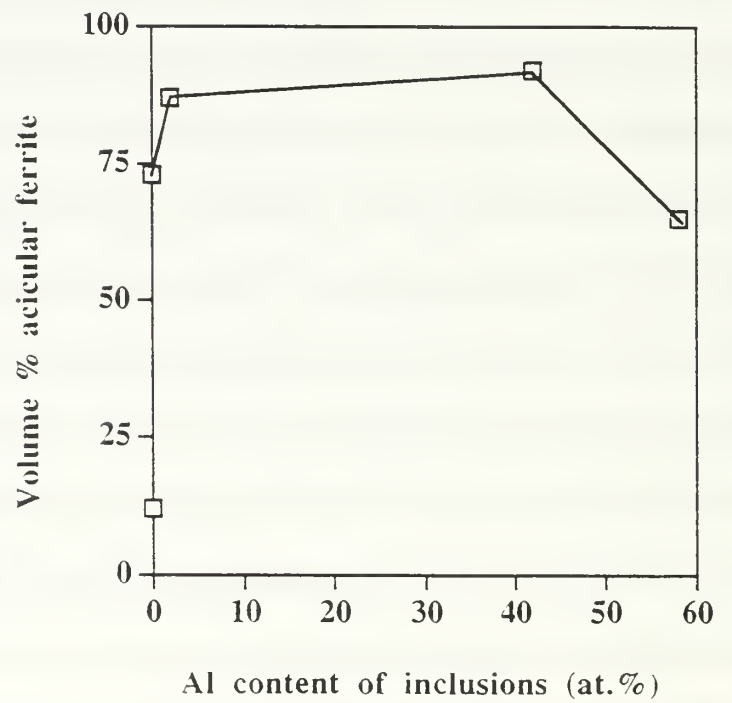


**Figure 4-14**. Volume percent acicular ferrite vs. atomic % aluminum inclusion content. (The errors for both axes are less than the symbol size)

Following the same procedure for titanium, Figure 4-15 is the volume percent of acicular ferrite vs. the amount (ppm) of titanium in the weld metal. This figure suggests that high levels of aluminum in the weld metal actually decreases the final volume percent of acicular ferrite. To really see the effect of titanium addition in a weld metal, the volume percent acicular ferrite is plotted against the atomic percent of titanium in the inclusions (Figure 4-16, note here the vertical errors are within the box). This graph clearly shows how titanium-containing inclusions dominates the issue of acicular ferrite formation. Weld metals rich in titanium oxide inclusions have a greater propensity of nucleating high levels of acicular ferrite.

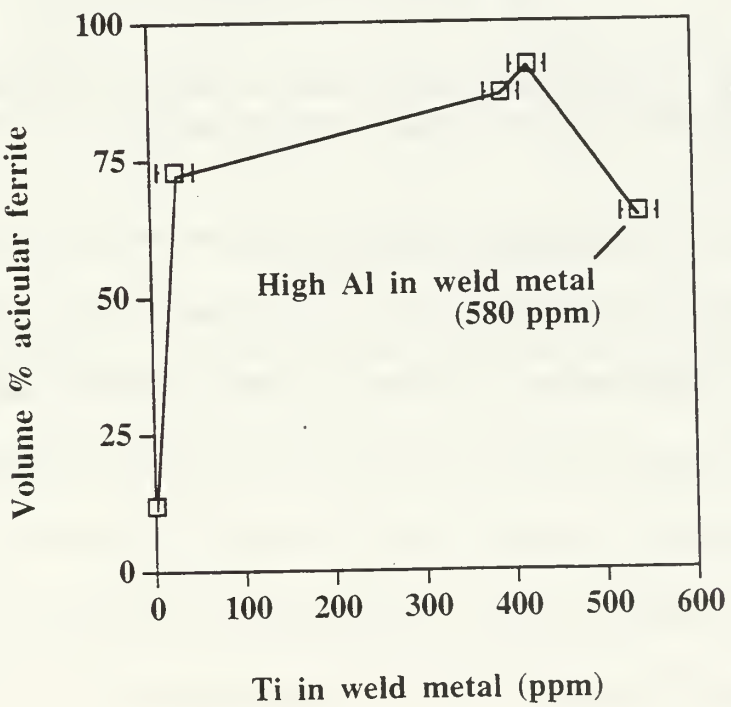


**Figure 4-15.** Volume percent acicular ferrite vs. weld metal titanium. (The errors in acicular ferrite content are less than the symbol size)

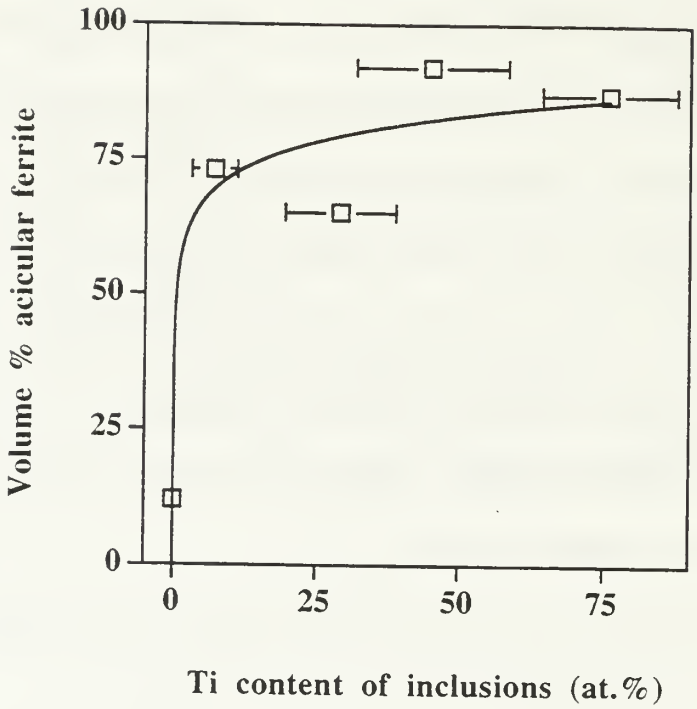


**Figure 4-16**. Volume percent acicular ferrite vs. atomic % titanium in inclusions. (The errors in acicular ferrite content are less than the symbol size)

Going back to the inclusion size distribution data portrayed in Figures 4-9 through 4-11, an interesting comprehensive result becomes apparent when comparing the volume percent acicular ferrite with the mean inclusion size from sample to sample (Figure 4-17). This figure goes against Zhang and Farrar [Ref. 40] suggestions regarding acicular ferrite forming inclusion size. For the five samples studied in the present work, the volume percent acicular ferrite increases with *decreasing* mean inclusion size. If you couple the results of the last few pages that titanium rich inclusions are strong acicular ferrite formers and that decreasing their mean inclusion size increases the acicular ferrite content in the weld metal, then it would seem that smaller titanium rich inclusions are stronger

acicular ferrite formers compared with larger inclusions which do not contain Ti. Indeed, plotting the mean inclusion size vs. the inclusions' atomic percent titanium, Figure 4-18 shows how inclusions rich in titanium actually decrease the mean inclusion size.

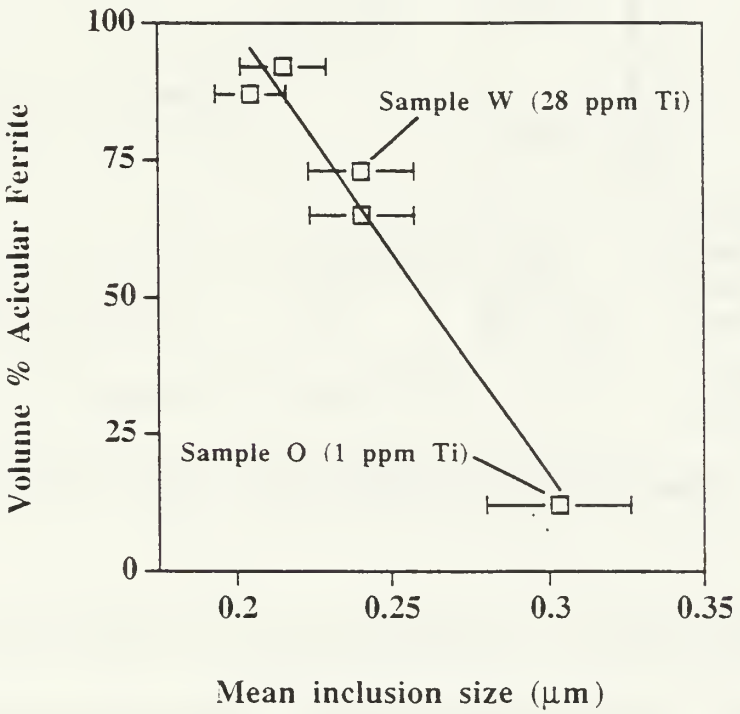


**Figure 4-17**. Volume % acicular ferrite vs. mean inclusion size. (The errors in acicular ferrite content are less than the symbol size)

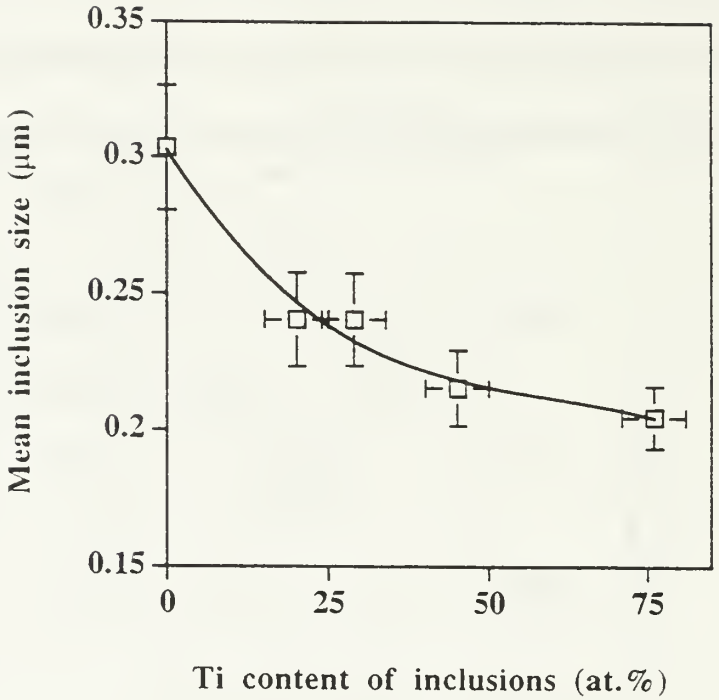


**Figure 4-18**. Mean inclusion size vs. atomic % titanium of inclusions.

These results seem to confirm the research of Gregg and Bhadesia [Ref. 15] and Fox et al. [Ref. 11] that titanium rich inclusions accelerate the nucleation of acicular ferrite. The mechanism(s) of acicular ferrite nucleation on these inclusions seems to occur as the initially titanium rich oxides ($TiO_2$ and $Ti_2O_3$) are reduced through deoxidation to TiO. TiO has good lattice matching for epitaxial growth, but more importantly, this deoxidation process appears to deoxidize the area immediately surrounding the inclusions creating an inclusion/matrix interface that has a strong chemical reaction for nucleation of acicular ferrite. Figure 4-19 is a sketch of the process.

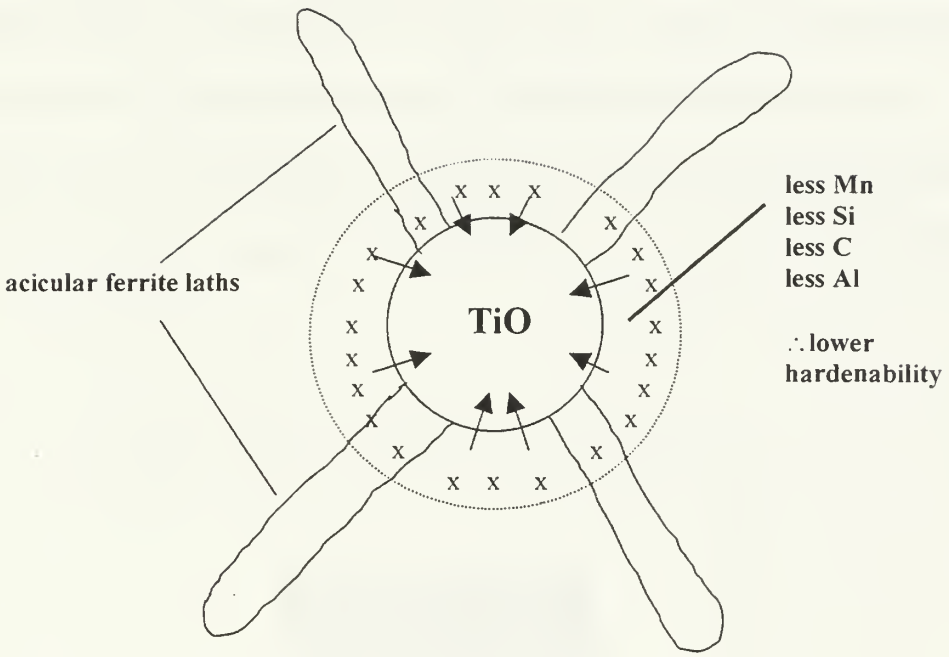


**Figure 4-19**. Sketch of the deoxidation process that accelerates AF formation.

## E. TEM RESULTS

Sample Z was analyzed using the Topcon 002B TEM/EDX. Although all five samples have been analyzed using the TEM [Ref. 39 and 50], sample Z resulted in the highest amount of acicular ferrite and the possibility exists of a strong acicular ferrite-forming compound. Carbon extraction replicas produced specimens of numerous inclusions with varying sizes. Figure 4-20 is a STEM (Scanning Transmission Electron Microscope) micrograph of a typical inclusion distribution in a carbon extraction replica.

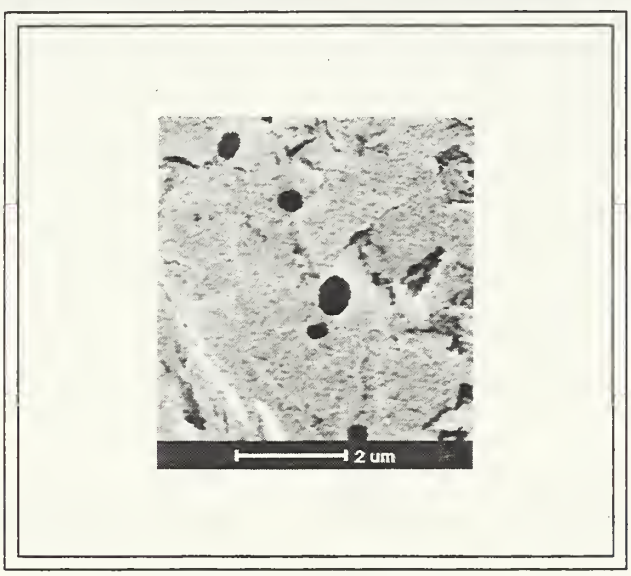


**Figure 4-20**. STEM micrograph of typical carbon extraction replica inclusions.

### 1. Inclusion MMZ1

Figure 4-21 is a STEM micrograph of a typical inclusion in sample Z with an EDX spectrum graph of the chemical composition also displayed. This typical inclusion produced a TEM/EDX analysis that displayed an almost 1/1 ratio of average atomic percent titanium to aluminum. The EDX analysis showed the inclusion was a mixture of titanium and aluminum (strong nickel counts appearing from the nickel grid) with small amounts of manganese, sulfur, silicon, iron, and copper. This suggests the main components of the inclusion were $Al_2O_3$ and TiO.

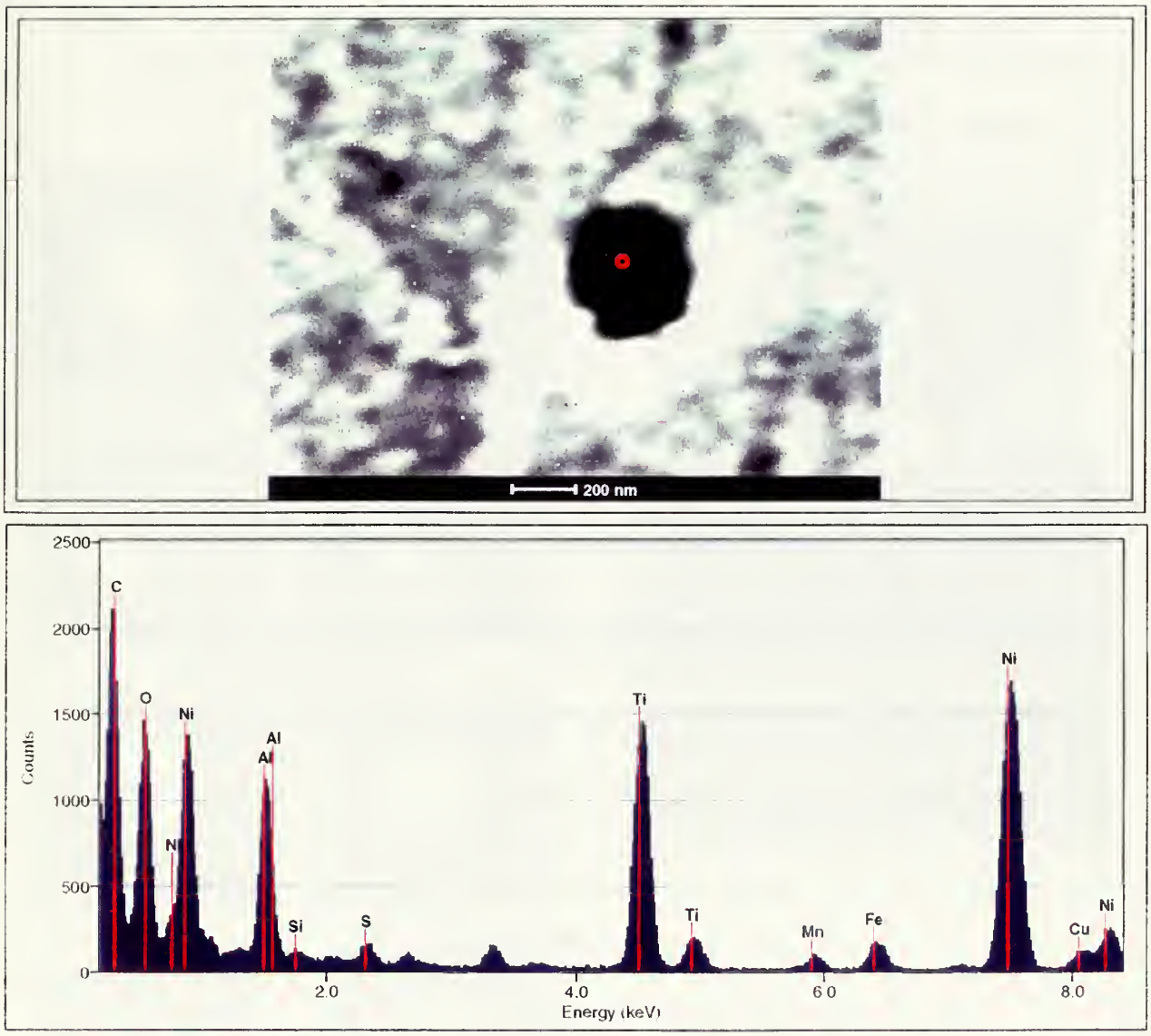


**Figure 4-21**. STEM micrograph and EDX spectrum of a typical inclusion in sample Z.

Further analysis of inclusion MMZ1 with a selected area diffraction (SAD) analysis (as in Figure 4-22) and EDX mapping clearly shows that this mixture of $Al_2O_3$ and TiO is uniform over the entire inclusion with a small cap of iron/copper sulfide on the lower right corner. Again from previous research and from the results of this work, this sample seems to have formed a new compound of $Al_2O_3$ and TiO. This is very significant and will be discussed in the next section.

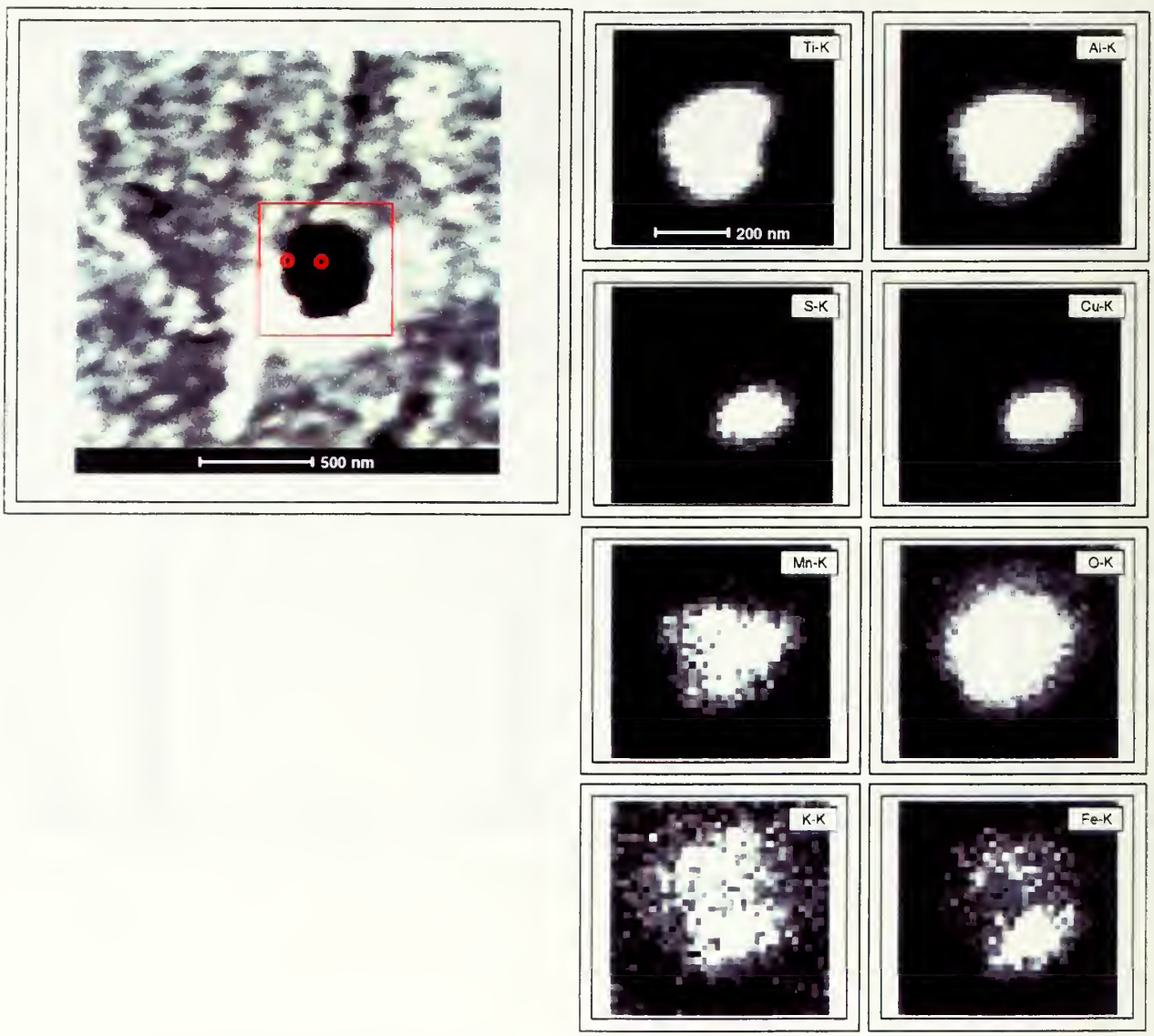


**Figure 4-22.** STEM micrograph and EDX maps of inclusion MMZ1.

A bright field TEM image was taken of inclusion MMZ1 as well as a selected area diffraction pattern (Figure 4-23). Analysis of the d-spacings and lattice parameters is still under investigation, but the diffraction pattern clearly displays a single crystal pattern. This adds credibility to the belief that sample Z inclusions are essentially a new compound of $Al_2O_3$ and TiO.

**Figure 4-23**. Bright field TEM image and diffraction pattern of MMZ1.

## 2. Inclusions MMZ2 and MMZ3

A final analysis was performed on two inclusions found in sample Z (MMZ2 and MMZ3) that were of different size. SAD and EDX mapping analysis (Figure 4-24) shows strong agreement with the inclusion MMZ1 in that the titanium and aluminum are uniformly distributed throughout the inclusion. The associated diffraction pattern (Figure 4-25) is similar to that obtained for inclusion MMZ1.

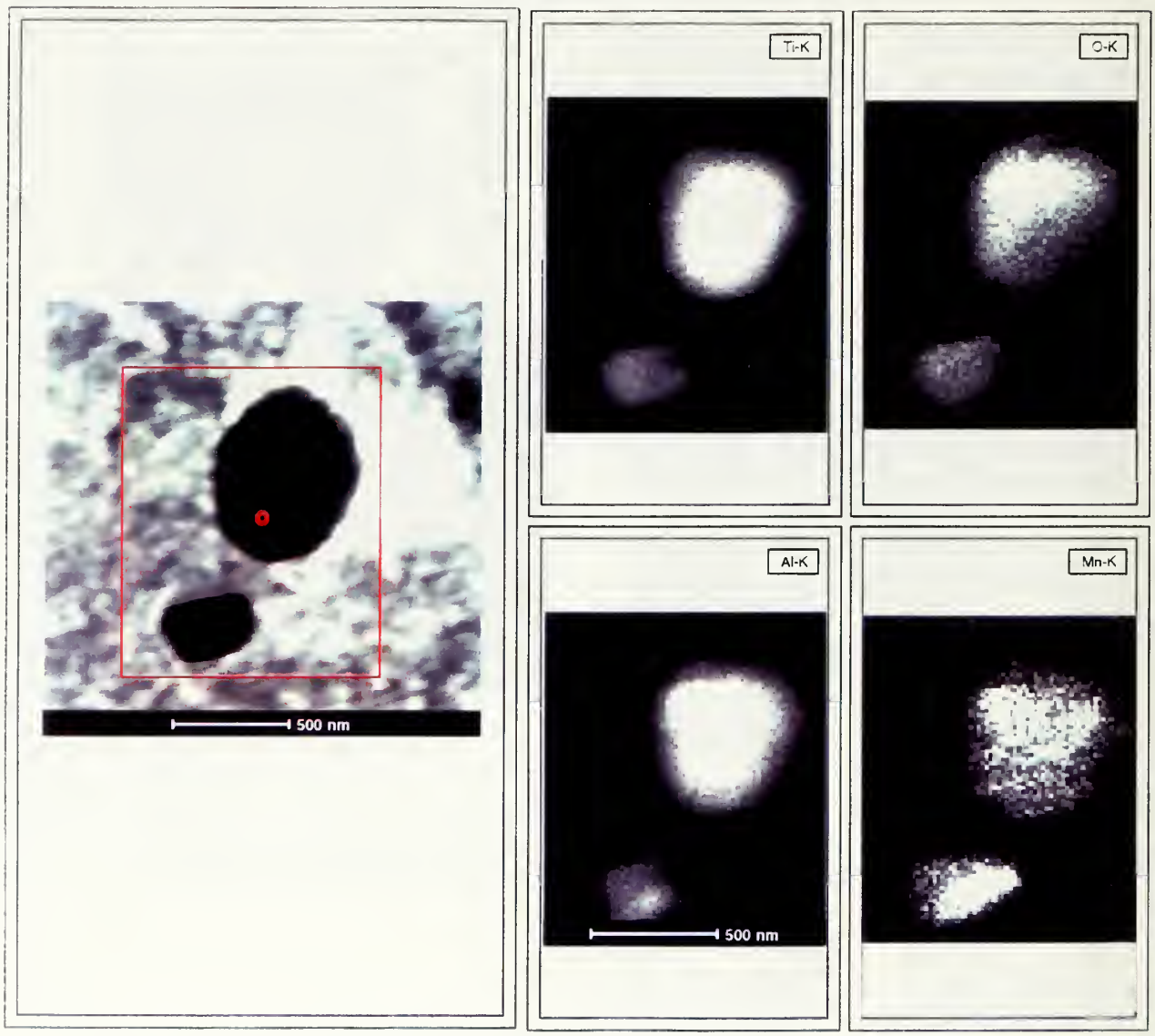


**Figure 4-24**. STEM micrograph and EDX mapping of inclusions MMZ2 and MMZ3.

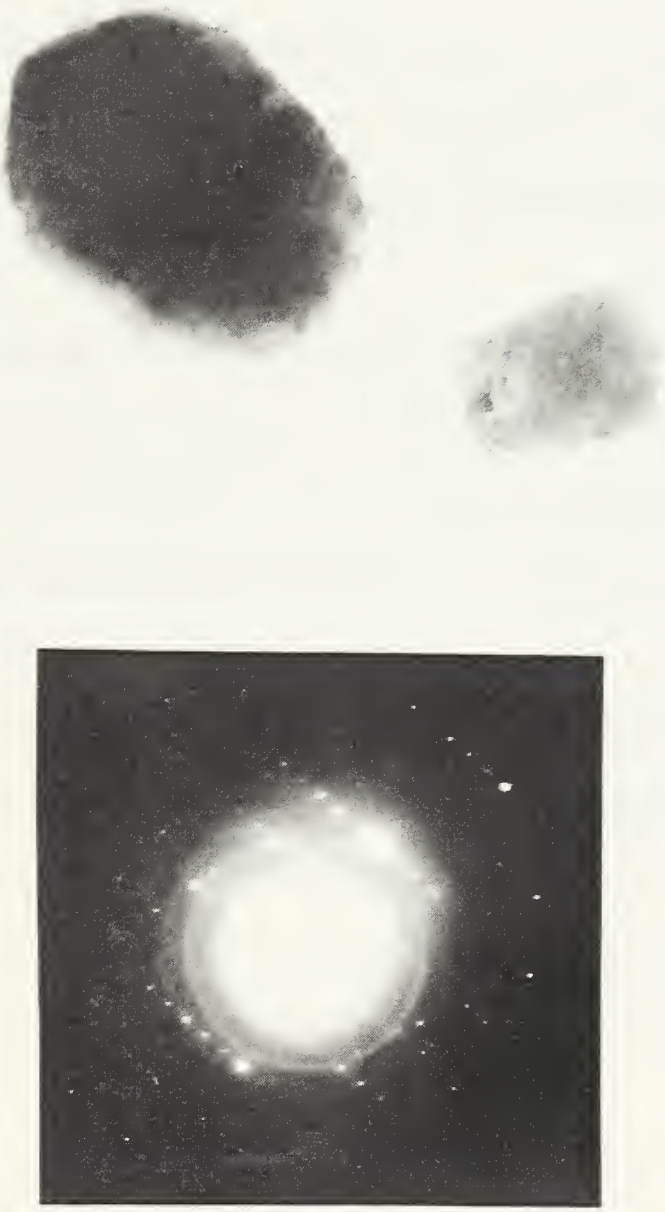

**Figure 4-25**. Bright field diffraction image and diffraction patterns of MMZ2 and MMZ3.

# V. SUMMARY

## A. CONCLUSIONS

The average prior austenite grain size was similar for all samples regardless of the amount of acicular ferrite obtained (exception being Sample O where little titanium and aluminum were added). This suggests that prior austenite grain size in these samples is large enough so that it does not have a major role in influencing acicular ferrite nucleation or growth.

The inclusion size distributions were slightly skewed to higher diameters with a mean inclusion size of 0.2253 +/- 0.02 μm. For all five samples studied, the volume percent acicular ferrite actually increases with decreasing mean inclusion size. All evidence suggests that smaller titanium-rich inclusions are the strongest acicular ferrite formers and actually accelerate its growth.

The mechanism by which titanium rich inclusions nucleate acicular ferrite appears to be through chemical reaction and possible epitaxial growth. The deoxidation of the initially titanium-rich oxides ($TiO_2$ and $Ti_2O_3$) produces a denuded/clean area immediately surrounding the now TiO dominate inclusion creating an inclusion/matrix interface (chemistry) and good lattice matching (epitaxial) for the nucleation of acicular ferrite.

Generating levels of titanium above 400 ppm in the weld metal, while keeping all other deoxidants at low levels produces large amounts of acicular ferrite for the samples studied in the present work.

All evidence (TEM/EDX and diffraction patterns) suggests obtaining a 1/1 ratio of atomic percent titanium to aluminum in the inclusions may result in a new compound $Al_2O_3$.TiO that further accelerates acicular ferrite nucleation and growth.

## B. SUGGESTIONS FOR FURTHER RESEARCH

Chemistry and crystallographic investigation of the inclusion/matrix interface needs to be performed to determine if epitaxy actually exists.

Additional diffraction analysis needs to be conducted on sample Z inclusions to determine the exact nature of this new one phase compound ($Al_2O_3$.TiO).

New methods to obtain thin inclusion matrix samples need to be developed by possibly ion thinning the hard inclusions to a point where inclusion matrix interfaces can be investigated by TEM.

New weld metal samples with levels of titanium above 400 ppm from different arc welding processes need to be investigated to see if the conclusions of the present work are still consistent.

## REFERENCES CITED


1. Kou, S., *Welding Metallurgy*, John Wiley and Sons, New York,1987.

2. Bhadesia, H.K.D.H., *Bainite in Steels*, The Institute of Materials, London, Chapter 10, 1990.

3. *Guidelines for Classification of Ferritic Steel Weld Metal Microstructural Constituents using the Light Microscope*. IIW Doc. No. IXJ-102-85.

4. Shewmon, P., *Transformations in Metals*, J. Williams Book Company, 1983.

5. Bhadeshia, H.K.D.H., "Control of Weld Metal Microstructure and Properties," *The Metallurgy, Welding, and Qualification of Microalloyed (HSLA) Steel Weldments*, American Welding Society, 1990.

6. Harrison, P.L. and Farrar, R.A., "Influence of Oxygen-Rich Inclusions on the Austenite-to-Ferrite Phase Transformations in high-strength-low-alloy (HSLA) Steel Weld Metals," *Journal of Materials Science*, 16:2218-2226, 1981.

7. *Metals Handbook Ninth Edition, Volume 6 Welding, Brazing and Soldering*, American Society of Metals, Metals Park, Ohio, 1983.

8. Evans, G.M., "The Effect of Titanium in Manganese-Containing SMA Weld Deposits," *Welding Journal*, 72: 123s,1993.

9. Bhadesia, H.K.D.H., *Bainite in Steels*, Institute of Metals, 1992.

10. Ito, Y., Nakanishi, M. and Komizo, Y., "Effects of Oxygen on Low Carbon Steel Weld Metal," *Metal Construction*, 472, 1982.

11. Fox, A.G., Clarke, A.L. and Franke, G.L., "The Effect of Small Changes in Flux MnO Content on the Microstructure and Mechanical Properties of Navy HY-100 Steel," *Welding Journal*, 1998.

12. Grong, Ø., Siewart, T.A., and Edwards, G.R., "Effects of Deoxidation Practice on the Transformation Behavior and Toughness of Steel Welds," *Welding Research Supplement to the Welding Journal*, 279s-288s, November 1986.

13. Babu, S.S. and Bhadesia, H.K.D.H., "Mechanism of the Transition from Bainite to Acicular Ferrite," *Materials Transactions*, JIM, 32, 679, 1991.

14. Grong, Ø., Kluken, A.O., Nylund, H.K., Dons, A.L. and Hjelen, J., "Catalyst Effects in Heterogeneous Nucleation of Acicular Ferrite," *Metallurgical Transactions*, A 26: 525-534, 1995.

15. Gregg, J.M. and Bhadesia, H.K.D.H., "Solid State Nucleation of Acicular Ferrite on Minerals Added to Molten Steel," *Acta Materiala*, 45: 739, 1997.

16. Ricks, R.A., Howell, P.R. and Barrite, G.S., "The Nature of Acicular Ferrite in HSLA Steel Weld Metals," *Journal of Materials Science*, 17: 732-740, 1982.

17. Barrite, G.S. and Edmonds, D.V., "The Microstructure and Toughness of HSLA Steel Weld Metals," *Proceedings on Advances in the Physical Metallurgy of Steels Conference*, The Metals Society, 126-135, 1981.

18. Brooksbank, D. and Andrews, K.W., "Stress Fields Around Inclusions and their Relation to Mechanical Properties," *Journal of the Iron and Steel Institute*, 210: 246-255, 1972.

19. Dallam, C.B. and Olson, D.L., "The Effects of Stress and Grain Size on Weld Metal Ferrite Formation," *Welding Journal*, 68: 198s-205s, 1989.

20. Edwards, G.R. and Liu, S., "Recent Developments in HSLA Steel Welding," *Proceedings of the First United States-Japan Symposium on Advances in Welding Metallurgy*, cosponsored by the American Welding Society, the Japanese Welding Society and the Japanese Welding Engineering Society and held June 7-8 1990 at San Francisco, CA, U.S.A and June 12-15 1990 at Yokohama, Japan: 213-292, 1990.

21. Abson, D.J., "Nonmetallic Inclusions in Ferritic Steel Weld Metals," *International Institute for Welding*, Document IX-1486-87, 1987.

22. Pargeter, R.J., "Investigation of Submerged Arc Weld Metal Inclusions," *Proceedings of an International Conference on the Welding Metallurgy of Structural Steels*, The Metallurgical Society, Warrendale, PA, 393-414, 1987.

23. Devillers, L., Kaplan, D., Marandet, B., Ribes, A. and Riboud, P.V., "The Effect of Low Level Concentrations of Some Elements on the Toughness of Submerged Arc Welded C-Mn Steels," *Proceedings of the Effects of Residual, Impurity and Microalloying Elements on Weldability and Weld Properties Conference: Paper 1*, The Welding Institute, Abington, U.K., 1983.

24. Mizuno, M., Tanaka, I. and Adachi, H., "Chemical Bonding at the Fe/TiX (X=C, N or O) Interfaces," *Acta Materialia*, 46:1637, 1998.

25. Strangwood, M. and Bhadesia, H.K.D.H., "The Mechanism of Acicular Ferrite Formation in Steel Weld Deposits," *Advances in Welding Science and Technology*, ASM, Metals Park, Ohio, 209-213, 1987.

26. Babu, S.S., David, S.A., Vitek, J.M., Kundra, K. and DebRoy, T., "Development of Macro- and Microstructures of C-Mn Low Alloy Steel Welds - Inclusion Formation," *Materials Science and Technology*, 11: 186-199, 1995.

27. Kluken, A.O., Grong, Ø. and Rorvik, G., *Metallurgical Transactions*, 21:2047-2058, 1990.

28. Muan, A. and Osburn, E.F., "Phase Equilibrium Among Oxides in Steelmaking," Addison-Wesley Publishing Company, 1965.

29. Bhatti, A.R., Saggese, M.E., Hawkins, D.N., Whiteman, J.A. and Golding, M.S., "Analysis of Inclusions in Submerged Arc Welds in Microalloyed Steels," *Welding Journal*, 63: 224s-230s, 1984.

30. Kiessling, R. and Lange, N., "Non-Metallic Inclusions in Steel," *The Metals Society*, 1978.

31. Komizo, Y. and Fukada, Y., "Toughness Improvement in Weld Metal of Carbon and HSLA Steels in Japan," Sumitomo Metal Industries, Ltd., 1986.

32. Fox, A.G., Eakes, M.W. and Franke, G.L. "The Role of Titanium in the Non-Metallic Inclusions which Nucleate Acicular Ferrite in the Submerged Arc Weld (SAW) Fusion Zones of Navy HY-100 Steel," *Welding Journal Research Supplement 75*, 330s, 1996.

33. Dowling, J.M., Corbett, J.M. and Kerr, H.W., "Observations on Inclusions and Acicular Ferrite Nucleation in Submerged Arc HSLA Welds in High Strength Low Alloy Steels," *Metallurgical Transactions*, 17: 1611-1623, 1986.

34. Mills, A.R., Thewlis, G. and Whiteman, J.A. "The Nature of Inclusions in Steel Weld Metals and Their Influence on the Formation of Acicular Ferrite," *Materials Science and Technology*, 3: 1051-1061, 1987.

35. Thewlis, G., "The Influence of Pipe Plate and Consumable Chemistry on the Composition, Microstructure and Toughness of Weld Metal," *Proceedings of Welding and Performance of Pipelines Conference: Paper 9*, The Welding Institute, Abington, U.K., 1986.

36. Cochrane, R.C. and Kelville, B.R., "Influence of Inclusion Morphology on Microstructure and Toughness of Submerged Arc Weldments," *Proceedings of the Steels for Line Pipe and Pipeline Fittings Conference*, The Metals Society, 51-60, 1981.

37. Terashima, H. and Hart, P.H.M., "Effect of Aluminum on C-Mn-Nb Steel Submerged Arc Weld Metal Properties," *Welding Journal*, 63, 173s, 1984.

38. Grong, O. and Matlock ,D.K., "Microstructural Developments in Mild and Low Alloy Steel Weld Metals," *International Metals Review*, 31(1): 27-48, 1986.

39. Walters, J., "Microchemical Analysis of Non-Metallic Inclusions in C-Mn Steel Shielded Metal Arc Welds by Analytical Transmission Electron Microscopy," Master's Thesis, Naval Postgraduate School, 1998.

40. Zhang, Z. and Farrar, R.A., "Role of Non-Metallic Inclusions in Formation of Acicular Ferrite in Low Alloy Weld Metals," Material Science and Technology, 12: 237, 1996.

41. Chuen, S.L.K., "The Role of Non-Metallic Inclusions in Controlling Weld Metal Microstructures in Niobium Miroalloyed Steels," PhD Thesis No T-2923, Colorado School of Mines, 1984.

42. St-Laurent, S., L'Esperance, G., "Effects of Chemistry, Density and Size Distribution of inclusions on the nucleation of Acicular Ferrite of C-Mn Steel Shielded-Metal-Arc-Welding Weldments," *Materials Science and Engineering*, Al49, 1992.

43. Cerjak, H., Letofsky, E., Pitoiset, X., Seiringer, A., *The Influence of the Microstructure on the Toughness of C-Mn Multi-Run-Weld Metals*, IIW-Doc Ix-1814-95, 1995.

44. Kluken, A.O., Grong, O. and Hjelen, J., "The Origin of Transformation Textures in Steel Weld Metals Containing Acicular Ferrite," *Metallurgical Transactions*, 22:657-663, 1991.

45. Williams, D.B. and Carter, C.B. *Transmission Electron Microscopy Volume 4*, Plenum Press, NY, Chapter 36, 632, 1996.

46. Fox, A.G. and Menon, E.S.K., *Proposal to the National Science Foundation*, November, 1998.

47. Zhang, S., Hattori, N., Enomoto, M., and Tarui, T., "Ferrite Nucleation at Ceramic Austenite Interfaces," *ISIJ International* 36: 1301, 1996.

48. Yamamoto, K., Matsuda, S., Haze, T., Chijiiwa, R. and Mimura, H., *Proceedings of a Conference on Residual and Unspecified Elements in Steel*, ASM International, OH, 1987.

49. Chijiiwa, R., Tamehiro, H., Hirai, M., Matsuda, H. and Mimura, H., "Extra-High Toughness Titanium Oxide Steel Plates for Off-Shore Structures and Line Pipe," *Offshore Mechanics and Artic Engineering (OMAE)*, ASME, Houston, TX, 5: 165, 1988.

50. Greene, M.K., "The Effects of Titanium on the Mechanical Properties of Shielded Metal Arc Welding (SMAW) of C-Mn Steels," Master's Thesis, Naval Postgraduate School, Monterey, Ca, 1997.

51. Franklin, A.G., *Joining Iron Steel Institute*, 207: 181-186, 1969.

52. Evans, G.M., and Bailey, N., "Metallurgy of Basic Weld Metal," Abington Publishing, Cambridge, U.K., 13:286, 1997.

## INITIAL DISTRIBUTION LIST

1. Defense Technical Information Center ..... 2
   8725 John J. Kingman Rd., STE 0944
   Ft. Belvoir, Virginia 22060-6218

2. Dudley Knox Library ..... 2
   Naval Postgraduate School
   411 Dyer Rd.
   Monterey, California 93943-5100

3. Naval/Mechanical Engineering, Code 34 ..... 1
   Naval Postgraduate School
   700 Dyer Rd., Bldg. 245
   Monterey, California 93943-5100

4. Department Chairman, Code ME/Mc ..... 1
   Department of Mechanical Engineering
   Naval Postgraduate School
   700 Dyer Rd., Bldg. 245
   Monterey, California 93943-5100

5. Dr. Alan G. Fox, Code ME/Fx ..... 2
   Department of Mechanical Engineering
   Naval Postgraduate School
   700 Dyer Rd., Bldg. 245
   Monterey, California 93943-5100

6. Dr. G. M. Evans, ..... 1
   34 Grenfell Park
   Parkgate
   South Wirral L64 TT United Kingdom

7. CPT Michael F. Mahony ..... 2
   3416 West Shore Rd.
   Warwick, Rhode Island 02886